Full-potential linear-muffin-tin-orbital calculations of the magnetic properties of rare-earth–transition-metal intermetallics. I. Description of the formalism and application to the series $R\mathrm{Co}_5$ (R=rare-earth atom)

K. Hummler and M. Fähnle
Institut für Physik, Max-Planck-Institut für Metallforschung, Heisenbergstrasse 1, 70569 Stuttgart, Germany
(Received 7 April 1995; revised manuscript received 5 July 1995)

For the series $R\mathrm{Co}_5$ (R=rare-earth atom) various parameters occurring in the two-sublattice model of rare-earth–transition-metal intermetallics (local magnetic moments, intersublattice exchange fields, crystal field parameters, as well as magnetic hyperfine fields and electric field gradients) are calculated within the framework of the local-spin-density approximation (LSDA) and the full-potential linear-muffin-tin-orbital theory. Special emphasis is given to a determination of the crystal field parameter A_2^0. It is shown that it is absolutely indispensable to include the $5p$ states at the R site into the valence band and to avoid any spherical approximation for the effective potential. The quantity A_2^0 depends on the orientation of the aspherical $4f$ charge density, in contrast to a basic assumption of the two-sublattice model. As a result, the experiments in general yield some kind of average effective values which are different for different experiments. Application of the LSDA introduces rather large uncertainties for A_2^0 which cannot be totally removed but at least drastically reduced by physically motivated measures.

I. INTRODUCTION AND BASIC CONCEPTS

A. Rare-earth–transition-metal intermetallics

Intermetallic compounds of rare-earth atoms and transition-metal atoms are of great importance both for the technological application as well as from the viewpoint of basic research. First, the most powerful permanent magnets are among this class of materials.[1,2] Second, they represent a big challenge for the electron theory, because their properties are determined by two totally different types of electronic states, i.e., the highly correlated and strongly localized $4f$ states of the rare-earth atoms (R) and the valence states of the transition-metal atoms which are comparatively weakly correlated and more delocalized. In the present paper we investigate systems for which the $4f$ states may be considered as core states. For these materials a variety of properties (local magnetic moments and hyperfine fields, intersublattice exchange couplings, electric field gradients, and crystal field parameters) have been calculated[3–5] by the *ab initio* electron theory in local-spin-density approximation (LSDA). Among these properties the crystal field parameters are most difficult to obtain because mathematically they are determined by an integral which involves the folding between the charge densities of the $4f$ states and the conduction electron states, which depends extremely sensitively on these two densities. In the present paper we therefore extensively discuss how reliably these charge densities may be obtained within the framework of the LSDA. The calculations are performed for the technologically important systems $R\mathrm{Co}_5$ and are based on the full-potential linear-muffin-tin-orbital theory (FLMTO). The paper is organized as follows. In Secs. I B and I C the standard model of rare-earth metals and the two-sublattice model of rare-earth intermetallics are discussed. In Sec. I D the basic formulas for the calculation of the crystal field parameters are given. Section II considers the computational details concerning the FLMTO method and the problems arising from the application of the LSDA. In Sec. III test calculations are performed for SmCo_5, and in Sec. IV the results for the whole series $R\mathrm{Co}_5$ are reported.

B. The standard model of rare-earth magnetism

The question whether the $4f$ states of the rare-earth metals are to be considered as core states or as band states has been discussed for many years. The general trend is that the localization of the $4f$ states is too weak in LSDA. Therefore, treating the $4f$ states as band states yields a too strong hybridization with the other valence states, and thus the density of states at the Fermi level is much too large.[6] To obtain good results for the ground state properties, especially for the cohesive properties, the $4f$ states therefore were treated as core states in many publications (see, for instance, Refs. 3, 7), i.e., it was assumed that the $4f$ shells in the rare-earth metals essentially retain an atomic character determined by Hund's rules and that there are no hybridization effects with other states. This model is called the standard model or ionic model of rare-earth metals.

It should be noted that the standard model is of course not able to account for all aspects of rare-earth magnetism. First, it is sometimes argued that the correct structure of the Fermi surface may only be obtained by taking into account the hybridization of a narrow and energetically high-lying minority spin f band with the transition-metal–like valence states. This was discussed for Gd by Singh,[8] a viewpoint, which, however, was criticized by Bylander and Kleinman[9] and by Ahuja *et al.*[10] Temmerman *et al.*[11] have shown that when including the self-interaction correction in an LSDA calculation for Pr the occupied f bands occur well below the bottom of the conduction bands, whilst the high-lying f bands hybridize strongly with the conduction states at E_F, creating flat d bands at the Fermi level and a Fermi surface in agreement with experiments. Experimentally, a particular mode of magnetic excitation in Pr recently found by inelastic

TABLE I. Test of the validity of the inequality (1) for various representatives of the series $R_2Fe_{14}B$. The values of Δ and S_R are from Ref. 14, the values of B_{ex} from Ref. 5, and the values of E_{cf} from Eq. (7) of Ref. 4 with data for J and α_J from Ref. 14, values for $\langle r^2\rangle_{4f}$ from Ref. 15, and with (Ref. 17) $A_2^0=300$ K/a$_0^2$ for the whole series.

	Pr	Nd	Sm	Tb	Dy	Ho	Er	Tm	Yb
$\frac{\Delta}{2\mu_B 2S^R B_{ex}}$	3.33	2.54	0.83	1.24	2.79	5.38	9.71	18.4	51.2
$\frac{2\mu_B 2S^R B_{ex}}{E_{cf}}$	3.08	9.7	10	10	7.3	16.2	11.7	3.3	1.5

neutron scattering experiments[12] also may be a hint towards hybridization effects between $4f$ and conduction-electron states. Second, and even more important, the properties of Ce compounds—especially those of the heavy fermion systems—can only be reproduced by taking into account the hybridization of the strongly correlated f states with the delocalized conduction states; see, for instance, Ref. 13.

In the present paper I and the following papers II and III, we assume that many properties of rare-earth intermetallics (the Ce compounds are excluded) can be essentially described by considering the $4f$ states as core states, and we discuss the problems related to the use of the LSDA for this situation. Furthermore, it is assumed that in the intermetallics all rare-earth atoms are in the trivalent state, i.e., that there are R^{3+} ionic cores.[3–5] This is by no means trivial, because most of the free rare-earth ions are divalent and the elemental rare-earth metals are trivalent except for Eu and Yb, but it is justified *a posteriori*[5] by the good agreement between the theoretical results and the experimental data for the magnetic moments.

C. An interaction hierarchy and the two-sublattice model

Although the standard model does not allow for a hybridization of the $4f$ states with the conduction electron states there are of course interactions between these two electronic systems which are responsible for most of the interesting physics of the rare-earth intermetallics. These are the exchange interactions between the respective spin densities and the electrostatic interaction between the respective charge densities. In the standard model it is assumed that the couplings within those two electronic subsystems are stronger than those between the two subsystems, so that the two subsystems retain their general properties in spite of the interaction. For instance, it is often assumed that for the $4f$ electrons the following hierarchy of interactions is fulfilled:

$$\Delta \gg (2\mu_B)(2S^R)B_{ex} \gg E_{cf}. \tag{1}$$

Here Δ is the lowest excitation energy from the ground state of the free R^{3+} ion, the second term in Eq. (1) represents the exchange-overall splitting of the R^{3+} multiplet level due to the exchange field B_{ex} imposed to the R^{3+} ion by the transition-metal sublattice (S^R is the projection of the total spin of the R^{3+} core on the quantization axis which is given by the total angular momentum $\mathbf{J}$), and E_{cf} is the crystal field interaction energy between the $4f$ charge density and all the other charges in the system. The first part of the inequality (1) ensures that there is no admixture of higher multiplet states to the ground state due to the exchange interactions with the conduction electron system, so that J is a good quantum number. The second part guarantees that there is no mixture of various M_J states due to the crystal field interaction, so that altogether the ground state is described by $(J,|M_J|=J)$. From Table I it becomes obvious that the first part of the inequality is not fulfilled for Tb and especially for Sm, so that in the latter case the exchange splitting probably leads to a mixture of different multiplet states. Nevertheless, in the present paper we mainly consider $SmCo_5$ and assume that the R^{3+} ion is basically in the ground state multiplet of the free R^{3+} ion. The reason for investigating $SmCo_5$ is the high technological importance and the fact that various other studies based on this assumption are at hand for comparison. The basic results of the present paper concerning the applicability of the LSDA and the validity of several assumptions of the two-sublattice model are *not* affected by these problems for Sm, however, the problems should be taken into account when comparing the theoretical data with the experimental results (Sec. IV C of paper II).

Based on the above discussed separation of the $4f$ states and the conduction electron states the two-sublattice mean-field model (see, for instance, Refs. 1, 5, 17) for the energy of the transition-metal sublattice (T) and the rare-earth sublattice (R) has been introduced,

$$E=-2\mu_B\sum_R \langle \mathbf{S}_R\rangle \mathbf{B}_{ex}(R)+E_{ani}^T+E_{cf}(R). \tag{2}$$

Here $2\mu_B\langle \mathbf{S}_R\rangle$ denotes the thermal average of the magnetic spin moment at the rare-earth site R, $\mathbf{B}_{ex}$ is the above introduced intersublattice exchange field (which is proportional to the thermal average $\langle \mathbf{S}_T\rangle$ of the transition-metal atom), E_{ani}^T is the magnetic anisotropy energy of the transition metal sublattice (which is usually described by a phenomenological ansatz with a few anisotropy parameters), and $E_{cf}(R)$ describes the magnetic anisotropy energy of the rare-earth ion at site R. The rare-earth anisotropy thereby originates from the electrostatic interaction of the aspherical $4f$ charge cloud with the crystal field produced by all the other charges in the system: when applying a strong external magnetic field oblique to the axis of the uniaxial anisotropy, the $4f$ moment and the magnetic moment of the transition-metal sublattice (which is coupled to the $4f$ moment via $\mathbf{B}_{ex}$) rotate out of the easy axis direction, the $4f$ charge density is corotated rigidly due to the strong spin-orbit coupling in the $4f$ core, the orientation of the aspherical $4f$ charge cloud in the crystal field becomes less favorable and the resulting increase in electro-

static energy is the magnetic anisotropy energy $E_{\rm cf}$. This energy may be represented by[1,4,5,16–19]

$$E_{\rm cf}=\sum_{n,m} A_n^m\langle\hat{C}_n^m\rangle_{4f}, \tag{3}$$

where the A_n^m denote the crystal field parameters determined by all charges in the system except for the charge of the $4f$ core under consideration and the $\langle\hat{C}_n^m\rangle$ are the expectation values of the $4f$ multipole moments, with

$$\langle\hat{C}_n^m\rangle_{4f}=\theta_{J,n}\langle r^n\rangle_{4f}\langle O_n^m\rangle_{4f}. \tag{4}$$

Here the $\theta_{J,n}$ are Steven's factors[18,19] which characterize the asphericity of the $4f$ charge density, $\langle r^n\rangle_{4f}$ are the $4f$ radial expectation values of r^n, and $\langle O_n^m\rangle_{4f}$ are the expectation values of Steven's operators.[18,19]

The basic assumption of the two-sublattice model is that $|\mathbf{B}_{\rm ex}|$, $|\langle\mathbf{S}_R\rangle|$, $|\langle\mathbf{S}_T\rangle|$, the anisotropy parameters entering $E_{\rm ani}^T$ as well as the parameters A_n^m, $\theta_{J,n}$, and $\langle r^n\rangle_{4f}$ do not depend on the orientation of the transition-metal moments and the rare-earth moments. Concerning the conduction electron sublattice, it indeed turned out[5] that the effective spin quantum number S_T is nearly independent of the relative orientation between the transition-metal sublattice and the rare-earth sublattice. On the other hand, although the coupling between the core- and the conduction-electron charge density is very small (see above), there will be small changes of the conduction electron states when rotating the aspherical $4f$ charge density, and because the crystal field parameters are very sensitive quantities they are considerably modified (Sec. III D), i.e., the A_n^m depend to some extent on the orientation of the $4f$ moment, in contrast to the assumption of the two-sublattice model. Concerning the $4f$ states, if the inequalities (1) were not fulfilled, the ground state could not be classified by the quantum numbers $(J,|M_J|=J)$ but there would be a mixture of states with different values of J and M_J depending on the relative orientation of the transition-metal moments and the rare-earth moments and on the orientation of the $4f$ charge density in the crystal. As a result, the magnetic properties of the $4f$ core (for instance S_R) and the asphericity of the $4f$ charge density would be different for different orientations, again in contrast to the assumption of the two-sublattice model. It is one of the objectives of the present paper to investigate the basic assumption of the two-sublattice model.

D. Crystal field parameters and intersublattice exchange couplings

From the electrostatic interaction energy between the $4f$ charge density $\rho_{4f}(\mathbf{r})$ at the rare-earth atom under consideration and the charge density $\rho(\mathbf{r}')$ produced by all the other charges in the system the following expression for the crystal field parameters was obtained[20]:

$$A_n^m=\frac{4\pi}{2n+1}\,c_n^m\int d^3r'\,\rho(\mathbf{r}')Z_{n,m}(\theta,\phi)\int dr\; r^2\,\frac{r_<^n}{r_>^{n+1}}\,\rho_{4f;n,m}(r)\;\Big/\int dr\; r^2 r^n\rho_{4f;n,m}(r). \tag{5}$$

Here the c_n^m are numerical factors (some of them are compiled in Ref. 21), Z_{nm} denotes the cubic harmonics (also called Tesseral harmonics, as in Ref. 19), $r_<$ $(r_>)$ is the smaller (larger) of $|\mathbf{r}'|$ and $|\mathbf{r}|$ and $\rho_{4f;n,m}$ are the radial expansion coefficients for the expansion of the aspherical $4f$ charge density into cubic harmonics

$$\rho_{4f}(\mathbf{r})=\sum_{n,m}\rho_{4f;n,m}(r)Z_{n,m}(\theta,\phi). \tag{6}$$

If we assume that the expansion coefficients $\rho_{4f;n,m}$ are independent of n and m, then we can replace in Eq. (5) the $\rho_{4f;n,m}(r)$ by one unique radial function $\rho_{4f}(r)$ and Eq. (5) reduces to Eq. (3) of Ref. 21, which was obtained already by Coehoorn[22] for A_2^0. It should be noted[4,5,20–22] that the often assumed proportionality between A_2^0 and the electric field gradient would only be valid if the $4f$ charge density ρ_{4f} was not overlapping with $\rho(\mathbf{r}')$.

For the calculation of $\rho(\mathbf{r}')$ two extreme models have been used in the past, the point-charge model which represents the metal by an assembly of fictitious point charges[1,23] outside the R atom under consideration and the valence model[4,5,22,24–27] which exclusively considers the contribution of the conduction states in the atomic sphere around this R atom (''valence contribution,'' the contribution from all the other charges outside the sphere is called ''lattice contribution''). Whereas the results of the first model depend extremely sensitively on the choice of the point charges,[23] the valence model together with the atomic-sphere approximation for the effective potential yielded[4,5,22,25–27] for the whole series $R_2Fe_{14}B$ values for A_2^0 in semiquantitative agreement with the experiments. Later, however, calculations[21,28,29] beyond the atomic-sphere approximation for $SmCo_5$ and $GdCo_5$ demonstrated that both the valence contribution and the lattice contribution of the remaining charges are important. Because both contributions are large and opposite in sign, the accurate calculation of A_2^0 depends extremely sensitively on the overlap of the charge densities $\rho(\mathbf{r}')$ and $\rho_{4f}(\mathbf{r})$ especially concerning the finest details of the tail of $\rho_{4f}(\mathbf{r})$. The main objective of Sec. III is to find out whether the LSDA is able to yield sufficiently accurate densities for a reliable determination of crystal field parameters. Treating the $4f$ states as band states in LSDA would certainly produce a too extended $4f$ charge density. Furthermore, it would lead to some hybridization with the other conduction electron states, and the decomposition of the total charge density into ρ_{4f} and ρ which is required for the discussion of crystal field parameters would be questionable. We therefore will treat the occupied $4f$ states as core states.

For a determination of the intersublattice exchange field $B_{\rm ex}$ we have used the method developed in Refs. 5, 26, 27,

30–33 via the *ab initio* calculations of the change ΔE in total energy upon inversion of the $4f$ moments.

II. COMPUTATIONAL DETAILS

A. Full-potential LMTO method

The *ab initio* calculations are performed within the framework of the LSDA with the exchange-correlation functional of Barth and Hedin.[34] The Kohn-Sham equations[35] are solved by a full-potential LMTO program based on a code originally developed by Savrasov and Savrasov,[36] which we have modified (see below) and for which we have written a spin-polarized version. In this program the crystal is partitioned into appropriately defined[36] atom-centered polyhedral cells, and for these cells inscribed muffin-tin spheres and circumscribed spheres centered at the atoms are defined. The basis functions, i.e., the linear-muffin-tin orbitals,[37] are constructed from Hankel functions for fixed energy $\varepsilon=\kappa^2$ centered at the basis atoms $\mathbf{R}$ in the unit cell described by the translation vector $\mathbf{t}$. These Hankel functions correspond to angular quantum numbers $L=(l,m)$. Inside its own muffin-tin sphere each Hankel function is smoothly augmented[37] by a respective linear combination of numerical radial functions, namely the solution $\phi_{\mathbf{R}l}(\varepsilon_{v\mathbf{R}L})$ of the Schrödinger equation for the effective potential averaged spherically around the considered basis atom $\mathbf{R}$ in the unit cell and for an appropriately chosen fixed energy $\varepsilon_{v\mathbf{R}L}$, as well as its energy derivative $\dot{\phi}_{\mathbf{R}l}(\varepsilon_{v\mathbf{R}L})$. Inside all the off-centered polyhedral cells around $\mathbf{R}'+\mathbf{t}'$ the Hankel functions are substituted by their expansions into spherical Bessel functions of angular momentum L' around the nuclei centered at $\mathbf{R}'+\mathbf{t}'$ up to a maximum angular momentum $l'=l_T$, and inside the respective off-site muffin-tin spheres the Bessel functions are smoothly augmented by linear combinations of $\phi_{\mathbf{R}'l'}$ and $\dot{\phi}_{\mathbf{R}'l'}$. Finally, from the so obtained LMTO's $\chi_{\kappa\mathbf{R}L}(\mathbf{r}-\mathbf{t}-\mathbf{R})$ the Bloch-transformed basis functions

$$\chi^{\mathbf{k}}_{\kappa\mathbf{R}L}=\sum_{\mathbf{t}} e^{i\mathbf{k}(\mathbf{R}+\mathbf{t})}\chi_{\kappa\mathbf{R}L}(\mathbf{r}-\mathbf{t}-\mathbf{R}) \tag{7}$$

are constructed, and then the eigenfunctions $\psi^{n\mathbf{k}}(\mathbf{r})$ (band index n, wave vector $\mathbf{k}$) are represented by a linear combination,

$$\psi^{n\mathbf{k}}(\mathbf{r})=\sum_{\kappa,\mathbf{R}}\sum_{l=0}^{l_B}\beta^{n\mathbf{k}}_{\kappa\mathbf{R}L}\chi^{\mathbf{k}}_{\kappa\mathbf{R}L}(\mathbf{r}), \tag{8}$$

where the l summation runs up to a maximum angular momentum l_B. Because of the use of the above discussed expansions of the LMTO's into functions defined with respect to centers of the polyhedral cells, the calculation of the Hamiltonian matrix and the overlap matrix may be reduced to the determination of radial integrals. The integrations within the muffin-tin spheres are simple, and the integrations within the interstitial space between the muffin-tin spheres and the geometrically complicated boundaries of the polyhedral cells are performed via a Chebyschev integration technique.[36] The electron density is calculated in the usual way from the eigenfunctions $\psi^{n\mathbf{k}}$, which are linear combinations of LMTO's up to an angular momentum $l=l_B$ but contain l' components up to l_T because of the expansions of the LMTO's. In most cases it is not necessary to keep track of all the resulting angular momentum components, but it is sufficient to terminate the expansion of the charge density and the effective potential up to $2l_w<2l_T$. In the original program version of Savrasov and Savrasov[36] the Hartree part $V^{H,\mathrm{ext}}_{l,m}$ of the effective potential inside the muffin-tin sphere around $\mathbf{R}$ originating from charges outside the respective on-site polyhedral cell is calculated via the multipole moments,

$$M_{\mathbf{R}'L'}\sim\int\rho(\mathbf{r}_{\mathbf{R}'})r^{l'}_{\mathbf{R}'}Y_{l'm'}(\hat{\mathbf{r}}_{\mathbf{R}'})d^3r_{\mathbf{R}'}, \tag{9}$$

where the integrations extend over the polyhedral cells centered at $\mathbf{R}'$ and the $Y_{l',m'}$ denote the spherical harmonics. Even though the asphericity of the charge density $\rho(\mathbf{r}_{\mathbf{R}'})$ is generally small, considerable multipole moments may be generated via the integration over a polyhedral cell if the geometry of this cell strongly deviates from a sphere. It turns out that for small angular momentum l the part $V^{H,\mathrm{ext}}_{l,m}$ of the Hartree potential,

$$V^{H,\mathrm{ext}}_{l,m}(r_{\mathbf{R}})\sim r^{l}_{\mathbf{R}}\sum_{\mathbf{R}',L'}S^{*\mathbf{k}=0}_{\mathbf{R}L;\mathbf{R}'L'}(\kappa=0)M_{\mathbf{R}'L'}/(2l'+1), \tag{10}$$

nevertheless converges rapidly with l' because the elements of structure matrix $S^{*\mathbf{k}=0}_{\mathbf{R}L,\mathbf{R}'L'}$ are small for small l and large l'. However, the higher-l components of $V^{H,\mathrm{ext}}_{l,m}$ converge only slowly with increasing l'. Concerning the total energy, it seems to converge rapidly when increasing l_W for low values of l_W, but when increasing l_W further, the total energy disapproves and it will come back close to the low-l_W value only for very large values of l_W. For quantities which are nearly exclusively determined by the small-l components of $V^{H,\mathrm{ext}}_{l,m}(\mathbf{r}_{\mathbf{R}})$ there is no convergence problem in Eq. (10). For the calculation of the crystal field parameters, however, the higher-l components are also relevant, and we therefore have introduced in our program an option to determine $V^{H,\mathrm{ext}}_{l,m}(\mathbf{r}_{\mathbf{R}})$ for $1>3$ directly via a three-dimensional numerical integration in real space. Because this is very time consuming we take this option only for the final steps in the self-consistency cycle, whereas for the early steps Eq. (10) is used.

We thus have defined the most important technical parameters of the method, namely the angular momentum cutoffs l_B, l_T, and l_W, the number and the values of different κ's in Eq. (8) and the values of different $\varepsilon_{v\mathbf{R}L}$. Because the crystal field parameters are very sensitive quantities, we have carefully checked the influence of all these technical parameters on the A^m_n. It turned out that the results were converged for $(l_B,l_T,2l_W)=(2,8,10)$. The influence of the other parameters is discussed below.

In the following we distinguish between core states, semicore states, and valence states. The core states are strongly localized within the own muffin-tin sphere and energetically well separated from the other states at the same atom, so that no hybridization occurs. The semicore states correspond to the states of a closed outer shell in an atom, which in a crystal exhibit some spatial overlap with states at other atoms, but because they are energetically well separated from other states they hybridize only with the states of the same

kind at neighboring atoms, yielding narrow semicore bands. They are described by the eigenfunctions (8) for just one value of l and just one value of κ^2. The related energy parameter $\varepsilon_{\nu\mathbf{R}L}$ is chosen in such a way that the function $\phi_{\mathbf{R}L}(\varepsilon_{\nu\mathbf{R}L})$ exhibits the same node structure as the corresponding state of the atomic outer shell. Finally, to allow for all hybridization effects among the valence states an eigenfunction of type (8) with different l components is used, and for an accurate description of the eigenfunction in the interstitial region generally various values of κ^2 are required. Again, the energy parameters are chosen according to the correct node structure (except for ϕ_3; see Sec. II B 2). All states experience the same effective potential, but the Hamiltonian matrix for the semicore states is separately diagonalized from the one of the valence states, and as a result the valence states are in general not orthogonal to the other states. It should be noted that in several full-potential linearized-augmented-plane-wave codes (FLAPW) the eigenfunctions for a semicore calculation contain the same angular momentum components as the eigenfunctions for a valence calculation but the energy parameters are chosen in such a way that for the two types of calculations a different node structure appears for each l channel.

In some systems the energy of the atomic outer shell states is rather close to the energy of the atomic valence states. Then both types of states should be included in the ansatz (8) in order to allow for possible hybridization effects in the crystal. This is the case for many rare-earth compounds, where the $5p$ states (which are core states in the free atom) are energetically close to the $6s$, $6p$, and $5d$ states of the rare-earth atom. It is therefore important (see Sec. III A) to include in the eigenfunction (8) $l=1$ states [i.e., p states with $5p$ character (three nodes in the muffin-tin sphere) and with $6p$ character (four nodes)]. This is technically possible if we evaluate the respective LMTO's $\chi^{\mathbf{k}}_{\kappa\mathbf{R}L}$ for two different values of κ^2. (It should be noted that in a FLAPW code this may be achieved[38] when supplementing the FLAPW basis set by localized orbitals.)

B. Problems related to the application of the LSDA

The standard model discussed in Sec. I C is based on the strict separation of the occupied $4f$ states and the conduction electron states. If there are considerable hybridization effects between these two states, the two-sublattice model is no longer valid. For instance, the assumption that the crystal field parameters are independent of the orientation of the $4f$ charge density then is definitely wrong. The first task for a test of the two-sublattice model therefore in principle would be to explore the hybridization effects, which is rendered difficult because of the following reasons: first, the energetics of the $4f$ states is not correctly described in the pure spin-density functional theory because of the lack of orbital polarization effects (Hund's second rule), and it is also badly described by the LSDA [even if the self-interaction correction is performed as in the paper of Temmerman *et al.*[11] there are problems related to the nonlinearity of the exchange-correlation potential in LSDA (Ref. 9)], so that altogether the small hybridization effects are difficult to study. Second, it is hard to estimate how strongly the two-sublattice model would be violated by these small hybridization effects. The only way to test for the two-sublattice model therefore is to adopt tentatively its basic assumption, i.e., to neglect these hybridization effects, to calculate the parameters of the model (for instance, B_{ex}, A_n^m, etc.) by the *ab initio* electron theory and to compare the theoretical results with the experimental data.

Even if there are no hybridization effects between the occupied $4f$ states and the conduction electron states there is of course a coupling between these two subsystems via the effective potential to which the exchange and spin densities of both subsystems contribute. It is known that although the energetics of the $4f$ core states is badly described by the LSDA, the charge and spin density is quite well reproduced. For instance, the $4f$ spin form factor of a free Gd^{3+} ion as calculated by the LSDA (Ref. 6) is in excellent agreement[39] with an experiment on ionic Gd_2O_3 and with mixed configuration Dirac-Fock calculations.[15] In this section we want to discuss how reliably the $4f$ core charge density and the conduction electron charge density can be obtained by the LSDA in a metal.

1. The 4f core

To account for the strong Hund's rule couplings in the $4f$ shell Brooks *et al.*[40] have fixed the occupation numbers $n^{\uparrow}_{4f}$ and $n^{\downarrow}_{4f}$ for the two spin channels in such a way that the sum corresponds to the total number of $4f$ electrons in the free R^{3+} ion,

$$n^{\uparrow}_{4f}+n^{\downarrow}_{4f}=n_{4f}(R^{3+}), \tag{11}$$

and the difference corresponds to the projection of the free-ion $4f$ spin moment along the direction of the total $4f$ moment,

$$n^{\uparrow}_{4f}-n^{\downarrow}_{4f}=2(g_J-1)J, \tag{12}$$

where J is the total angular momentum quantum number and g_J denotes Landé's factor. Adopting a spherical approximation for the $4f$ charge density ρ_{4f} and the $4f$ magnetization density m_{4f} they arrived at

$$\rho_{4f}(r)=\frac{e}{\sqrt{4\pi}}[n^{\uparrow}_{4f}|\varphi^{\uparrow}_{4f}(r)|^2+n^{\downarrow}_{4f}|\varphi^{\downarrow}_{4f}(r)|^2]Z_{00}, \tag{13}$$

where the $\varphi^{\uparrow\downarrow}_{4f}$ are the radial functions for the $4f$ core as obtained from the LSDA calculation, subject to the constraints (11) and (12) and normalized according to

$$\int r^2 dr|\varphi^{\uparrow\downarrow}_{4f}(r)|^2=1, \tag{14}$$

as well as

$$m_{4f}(r)=\frac{\mu_B}{\sqrt{4\pi}}[n^{\uparrow}_{4f}|\varphi^{\uparrow}_{4f}(r)|^2-n^{\downarrow}_{4f}|\varphi^{\downarrow}_{4f}(r)|^2]Z_{00}. \tag{15}$$

To account for the asphericity of the $4f$ core, we can go beyond the constraints of Brooks *et al.*[40] and fix in addition the asphericity numbers $n^{\uparrow,J}_{4f;2l,0}$ and $n^{\downarrow,J}_{4f;2l,0}$ in

$$\rho_{4f}(\mathbf{r}) = e\sum_{l=0}^{3} [n^{\uparrow,J}_{4f;2l,0}|\varphi^{\uparrow}_{4f}(r)|^2 + n^{\downarrow,J}_{4f;2l,0}|\varphi^{\downarrow}_{4f}(r)|^2] Z^{J}_{2l,0}(\vartheta,\varphi) \tag{16}$$

and the corresponding expression for $m_{4f}(\mathbf{r})$. Here the $Z^{J}_{2l,0}$ denote the cubic harmonics for the polar axis parallel to the total angular momentum $\mathbf{J}$ of the $4f$ core. The $n^{\uparrow\downarrow,J}_{4f;2l,0}$ are fixed to the numbers which are obtained for a free R^{3+} ion, adopting the Russel-Saunders coupling scheme and representing the many-particle wave function of the $4f$ core by a Slater determinant of the single-particle wave functions for the spherically averaged effective potential with $\varphi^{\uparrow,\downarrow}_{4f}(r)$ for the radial part, respectively. Transforming to a system with polar axis parallel to the external z axis, we arrive at

$$\rho_{4f}(\mathbf{r}) = \sum_{n,m} \underbrace{e[n^{\uparrow}_{4f;n,m}|\varphi^{\uparrow}_{4f}(r)|^2 + n^{\downarrow}_{4f;n,m}|\varphi^{\downarrow}_{4f}(r)|^2]}_{\rho_{4f;n,m}(r)} Z_{n,m}(\vartheta,\varphi), \tag{17}$$

with $n^{\uparrow,\downarrow}_{4f;0,0} = n^{\uparrow,\downarrow}_{4f}/\sqrt{4\pi}$, which is used when calculating the effective potential. The square bracket can be identified with the radial expansion coefficients $\rho_{4f;n,m}(r)$ occurring in Eq. (6). Assuming that the functions $\varphi^{\uparrow}_{4f}(r)$ and $\varphi^{\downarrow}_{4f}(r)$ are identical and given by $\varphi_{4f}(r)$, we arrive at

$$\rho_{4f;n,m}(r) = e(n^{\uparrow}_{4f;nm} + n^{\downarrow}_{4f;n,m})|\varphi_{4f}(r)|^2, \tag{18}$$

and with the same assumption the sum of occupation numbers can be obtained from Eq. (4) as

$$n^{\uparrow}_{4f;n,m} + n^{\downarrow}_{4f;n,m} = \theta_{J,n}\langle O^{m}_{n}\rangle_{4f}. \tag{19}$$

Equation (17) and the corresponding equation for the magnetization density will be used in Sec. III as constraints for the self-consistent calculation. For the calculation of A^{m}_{n} according to Eq. (5) we partly take into account that $\varphi^{\uparrow}_{4f}$ and $\varphi^{\downarrow}_{4f}$ are slightly different, and we therefore replace $|\varphi_{4f}|^2$ by a weighted average over $|\varphi^{\uparrow}_{4f}|^2$ and $|\varphi^{\downarrow}_{4f}|^2$, arriving at the expression

$$\rho_{4f;n,m}(r) \sim (n^{\uparrow}_{4f;n,m} + n^{\downarrow}_{4f;n,m}) \frac{n^{\uparrow}_{4f}|\varphi^{\uparrow}_{4f}|^2 + n^{\downarrow}_{4f}|\varphi^{\downarrow}_{4f}|^2}{n^{\uparrow}_{4f} + n^{\downarrow}_{4f}}. \tag{20}$$

Finally, we have to select boundary conditions for the determination of $\varphi^{\uparrow,\downarrow}_{4f}(r)$ by the solution of the radial Kohn-Sham equation. To do this, the true effective potential, spherically averaged in the muffin-tin sphere, is continued beyond the muffin-tin sphere by

$$V^{\mathrm{av}}_{\mathrm{eff}} = \frac{a}{r} + b, \tag{21}$$

where the coefficients a and b are chosen in such a way that the potential is continuous and has a continuous radial derivative. If we impose atomic boundary conditions at infinity, the function $\varphi^{\uparrow,\downarrow}_{4f}(r)$ is too far extended to correspond to a core situation with no hybridization, i.e., we have to localize $\varphi^{\uparrow,\downarrow}_{4f}(r)$ in some way. To do this, Richter *et al.*[21] introduced a localization potential which is steeper than $V^{\mathrm{av}}_{\mathrm{eff}}$ for large distances, yielding a localization which, however, depends on the explicit form of the localization potential. Steinbeck *et al.*[41] represented the true effective crystal potential by a superposition of aperiodic on-site potentials and included the self-interaction correction (SIC) (see, for instance, Ref. 11) to the LSDA when determining $\varphi^{\uparrow,\downarrow}_{4f}(r)$ in such an on-site potential. The deconvolution of the crystal potential into on-site potentials is of course not unique, but Steinbeck *et al.* argued that because of the stronger localization of the SIC wave functions as compared to the LSDA wave functions the functions $\varphi^{\uparrow,\downarrow}_{4f}(r)$ depend only slightly on the detailed form of the on-site potential (we give a comment on this point in Sec. III E 1). However, this does not mean that the $4f$ wave functions are determined without any arbitrariness, because already the calculation of the wave functions in a nonperiodic potential instead of the periodic crystal potential introduces an arbitrariness: we are convinced that an LSDA-SIC band calculation in the true crystal potential for the occupied $4f$ states would lead to more expanded wave functions. In our calculations, we prescribe a localization sphere with radius $R_{4f,\mathrm{loc}}$ which is between the muffin-tin sphere and sphere circumscribing the polyhedral cell. The degree of localization is controlled by the value of $R_{4f,\mathrm{loc}}$ and by the logarithmic derivative D_{4f} at the sphere boundary. For $D_{4f} = -\infty$ the wave function vanishes at $R_{4f,\mathrm{loc}}$. Brooks *et al.*[40] have argued that the function $\varphi^{\uparrow,\downarrow}_{4f}(r)$ is probably better described within the localization sphere by imposing a finite negative D_{4f}, for instance $D_{4f} = -l-1 = -4$ which would correspond to the energy of the center of a hypothetical $4f$ band. Our guess is that the $4f$ wave function is slightly more expanded than the one of a free R^{3+} ion, but that it is quite similar to this. We therefore choose $R_{4f,\mathrm{loc}}$ and D_{4f} in such a way that the radial expectation values $\langle r^n\rangle_{4f}$ occurring in Eq. (5) for the A^{m}_{n} are close to those obtained by Dirac-Fock calculations[15] for the free R^{3+} ion. From Table II it becomes obvious that in $SmCo_5$ this is the case for $D_{4f} = -\infty$ and $3.46\ a_0 \leqslant R_{4f,\mathrm{loc}} \leqslant 4.10\ a_0$ (the radius of the muffin-tin sphere is $3.14\ a_0$). The dependence of $\langle r^n\rangle_{4f}$ on the choice of the boundary conditions is of course not surprising. However, it will be shown in Sec. III E 1 that the crystal field parameter A^{0}_{2} depends extremely sensitively on the choice of D_{4f}, $R_{4f,\mathrm{loc}}$. This is really shocking and demonstrates that within the framework of an LSDA calculation one has to make an additional assumption guided by physical intuition for an appropriate choice of the boundary conditions. As outlined above we think that the best choice is the one for which the values of $\langle r^n\rangle_{4f}$ are close to the Dirac-Fock values for the free R^{3+} ion.

2. The valence states

Having described the occupied $4f$ states as core states, we include in the basis set for the valence only s, p, and d functions. Nevertheless, the decomposition of the so-obtained valence states into different angular momentum contributions with respect to the center of the muffin-tin sphere also contains f contributions. This becomes obvious from the one-center expansions of the Hankel functions into spherical Bessel functions j_l discussed in Sec. II A. Augmenting the Bessel function j_3 by a radial f function ϕ_{4f} with an energy which corresponds to the center of gravity of the occupied valence band unfortunately yields (due to the wrong energetics of the $4f$ states in LSDA) an f function

TABLE II. Influence of $R_{4f,\mathrm{loc}}$ and D_{4f} on $\langle r^n\rangle_{4f}$ (in units of a_0^n) for $SmCo_5$. The column DF exhibits the results of a Dirac-Fock calculation (Ref. 15) for the free Sm^{3+} ion.

			$R_{4f,\mathrm{loc}}[a_0]$				
			3.14	3.46	3.78	4.10	DF
	$-\infty$	$\langle r^{-3}\rangle_{4f}$	6.90	6.79	6.75	6.72	6.89
		$\langle r^{2}\rangle_{4f}$	0.98	1.03	1.06	1.08	0.97
		$\langle r^{4}\rangle_{4f}$	2.03	2.44	2.66	2.89	2.26
		$\langle r^{6}\rangle_{4f}$	6.82	9.84	11.7	14.0	10.6
	$-l-1=-4$	$\langle r^{-3}\rangle_{4f}$	6.69	6.65	6.64	6.63	6.89
D_{4f}		$\langle r^{2}\rangle_{4f}$	1.09	1.13	1.15	1.17	0.97
		$\langle r^{4}\rangle_{4f}$	2.82	3.30	3.52	3.81	2.26
		$\langle r^{6}\rangle_{4f}$	12.5	17.6	20.4	24.5	10.6
	0	$\langle r^{-3}\rangle_{4f}$	6.23	6.34	6.39	6.41	6.89
		$\langle r^{2}\rangle_{4f}$	1.40	1.41	1.40	1.42	0.97
		$\langle r^{4}\rangle_{4f}$	5.30	6.08	6.28	6.92	2.26
		$\langle r^{6}\rangle_{4f}$	32.0	45.4	50.8	63.7	10.6

which looks very much like the one of a $4f$ core state, i.e., it exhibits a maximum in the muffin-tin sphere (Fig. 1). Because the valence states are not orthogonal to our core states, an unrealistically large $4f$ contribution to the valence states arises. Although its weight is still small compared to the s, p, and d contributions it deteriorates the results for A_n^m because of the folding of the $4f$ core density $\rho_{4f}(\mathbf{r})$ and the density $\rho(\mathbf{r}')$ in Eq. (5). To get rid of this problem,[42] we augment the Bessel function j_3 in the muffin-tin sphere by a $4f$ radial function ϕ_{4f} with negative energy. As shown in Fig. 1, the maximum of ϕ_{4f} in the muffin-tin sphere gradually vanishes when decreasing the energy and for moderate negative energies ϕ_{4f} is similar to the Bessel function j_3 and to a typical nodeless augmentation function of an almost unoccupied valence state. It is not appropriate to choose extremely low values of the energy, because then the wave function is steepened very sharply at the surface of the muffin-tin sphere, and a very high ϕ_{4f} contribution would be required to obtain the continuation to the f Bessel function outside the muffin-tin sphere. The influence of the $4f$ augmentation energy on the crystal field parameters is discussed in Sec. III E 2.

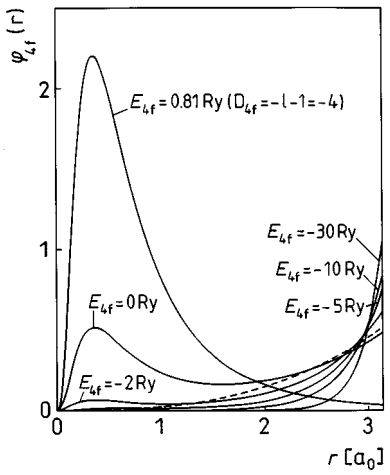

FIG. 1. $\phi_{4f}(r)$ for various augmentation energies in $SmCo_5$. The broken line is the Bessel function j_3 for $\kappa^2=0.4$ Ry.

III. TEST CALCULATIONS FOR $SmCo_5$

$SmCo_5$ crystallizes in the $CaCu_5$ structure with one Sm site ($1a$) and two crystallographically different Co sites ($3g$ and $2c$). The calculations were performed for experimental lattice parameters ($a=9.4563$ a_0, $c/a=0.7932$). For the Brillouin zone integration we used the tetrahedron method with the correction of Blöchl *et al.*[43] The results were satisfactorily converged for 40 k points in the irreducible part of the Brillouin zone and for $(l_B,l_T,2l_w)=(2,8,10)$. In the following we discuss the influence of various other parameters and details of the calculations. It thereby should be noted that when testing for the influence of one of these parameters, it is not always required to converge the results with respect to all the other parameters. This must be taken into account when comparing the data of the following tables and figures. Except for Sec. III C we assume for the calculation of the effective potential that the $4f$ charge density is spherically symmetric [Eq. (13)].

A. Subdivision into various energy panels and augmentation energies

The energetics of the states at the Sm $1a$ site and the Co $2c$ site is represented in Fig. 2. The highest true core states are the Sm-$4d$ and the Co-$3s$ states. All the states which are higher in energy represent band states which are labeled by their dominant contributions, and the centers of gravity of the various contributions are indicated by the full horizontal lines. In Table III we represent the results of three different calculations of the crystal field parameters A_n^m and the largest component V_{cc} of the diagonalized electric field gradient at the Sm site. The calculations differ by allowing for the hybridization among the electronic states within different subsets of the various electronic states shown in Fig. 2. The Hamiltonian matrices for the different subsets are di-

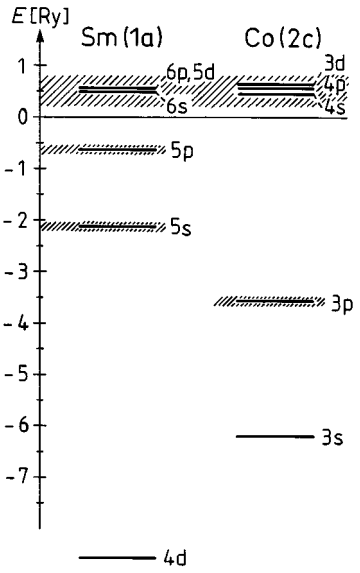

FIG. 2. Energetics of the states of the Sm $1a$ site and the Co $2c$ site in $SmCo_5$ (see text).

agonalized separately (Sec. II A), and the corresponding eigenvalues define the corresponding energy panels. In calculation A the $6s$, $6p$, and $5d$ states of Sm and the $4s$, $4p$, and $3d$ states of Co are treated as band states (with $\kappa^2=0.4$ Ry), and all the other states are core states. Calculation B considers the same band states, but the $5s$ and $5p$ states of Sm and the $3p$ states of Co are treated as separate semicore states, respectively. Finally, in calculation C the $5p$ state of Sm, which is energetically close to the $6s$, $6p$, $5d$ states is not considered as a semicore state, but it is included together with the $6s$, $6p$, and $5d$ states in the band calculation (with $\kappa^2=-0.9$ Ry; see Sec. II A). Table III shows that calculations A and B yield very similar results, but that it is really essential for the determination of A_2^0 and V_{cc} to include the $5p$ states of Sm into the valence band as in calculation C. In contrast to the higher-order crystal field parameters, which are mainly determined by the lattice contribution originating from charges outside the muffin-tin sphere, the quantities A_2^0 and V_{cc} exhibit strong valence contributions from the charges inside the muffin-tin sphere of the Sm atom, and these contributions are strongly influenced by the hybridization effects between the $5p$ states and the other valence states. It should be noted that the change in going from column A to B in Table III is opposite in sign to the contribution of the $5p$ semicore states in Refs. 28, 29. This might result from a slightly different meaning of the semicore treatment between FLMTO and FLAPW (see Sec. II A), or from the fact that when going from A to B we simultaneously switch from the treatment of the $5s$ states at Sm and of the $3p$ states at Co as core states to a treatment as semicore states, whereas in Refs. 28, 29 these states seem to be treated as core states.

TABLE III. Influence of the subdivision into various energy panels on the crystal field parameters A_n^m (total as well as valence and lattice contributions) and the electric field gradient V_{cc} at the Sm site (without the contribution from the $4f$ core); see text.

	A	B	C
$A_2^0[\mathrm{Ka}_0^{-2}]$	−377	−411	−246
Valence	−1568	−1607	−1447
Lattice	1191	1196	1201
$A_4^0[\mathrm{Ka}_0^{-4}]$	−10.4	−9.7	−9.6
$A_6^0[\mathrm{Ka}_0^{-6}]$	0.23	0.23	0.22
$A_6^6[\mathrm{Ka}_0^{-6}]$	−9.2	−9.0	−8.9
V_{cc}(Sm) $[10^{21}\ \mathrm{V\ m^{-2}}]$	20.0	19.7	8.7

When including the $5p$ states in the valence band, the results become virtually independent (except for the $4f$ states; see Sec. III E 2) of the energy parameters $\varepsilon_{\nu\mathbf{R}L}$ at which we evaluate $\phi_{\mathbf{R}L}$ and $\dot{\phi}_{\mathbf{R}L}$ (Sec. II A). We use in the following calculations for these parameters the energies κ^2 for the case $l>l_B$ and the respective centers of gravity of the occupied part of the l-projected band for the case $l\leqslant l_B$. When including only the $6p$ states in the valence band, the results depend critically (especially for multi-κ calculations) on the choice of the $6p$ augmentation energy. The reason is that the function $\phi_{\mathbf{R}L}(r)$ for the Sm site with $l=1$ exhibits near the lower band edge of the valence band a change of the number of nodes from 4 (“$6p$”) to 3 (“$5p$”). Altogether, this demonstrates that the inclusion of the $5p$ states in the valence band is indispensable, and this statement will be further underpinned by the comparison between theoretical and experimental results (Sec. IV).

B. Values of the kinetic energy parameters κ^2

For a good representation of the wave function in the interstitial space (Sec. II A) Bloch functions $\chi^{\mathbf{k}}_{\kappa\mathbf{R}L}$ [Eq. (7)] for various values at κ^2 are required in Eq. (8). This is clearly demonstrated by the dependence of A_2^0 on the choice of κ^2 in a one-κ calculation: varying κ^2 between 0.2 Ry and 0.5 Ry changes the value of A_2^0 by nearly a factor of 2. We therefore have to check convergence with respect to the number and values of κ^2. It thereby should be noted that we cannot use unlimited many values of κ^2, because this would induce numerical instabilities due to the overcompleteness of the basis set. Generally, the difference between various κ^2 values should be larger than 0.2 Ry. Table IV represents the results for different numbers of included κ^2 values. (Please note that for the one-κ calculation the $5p$ states cannot be included in the band calculation; see Sec. II A.) Already for the three-κ calculation the results are more or less independent of the detailed values of κ_i^2.

C. Asphericity of the effective potential

In calculations[4,5,22,25–27] based on the atomic-sphere approximation (see Sec. I D), the self-consistent effective potential is spherically averaged in each atomic sphere. Then, the eigenfunctions are evaluated for this potential by one further iteration step, yielding the aspherical valence-charge density. The feedback of the asphericity of the charge density on the effective potential is neglected. In the OLCAO calculations[21,41] the effective potential is constructed from overlapping extended site potentials, but for each site potential the intra-atomic asphericity is again quenched by azimuthal averaging over the site charge density during the iterations. To investigate the feedback of the asphericity of the charge density on the effective potential, we performed a

TABLE IV. Test of convergence with respect to the number of κ^2 values for A_n^m, V_{cc} at the Sm site (without $4f$ contribution), total moment μ_{tot}, the energy difference ΔE from which the intersublattice exchange field B_{ex} is calculated, and the total energy of the unit cell. The values of κ^2 are $\kappa_1^2=0.4$ Ry (one κ); $\kappa_1^2=-0.9$ Ry, $\kappa_2^2=0.4$ Ry (two κ); $\kappa_1^2=-0.9$ Ry, $\kappa_2^2=0.1$ Ry, $\kappa_3^2=0.7$ Ry (three κ); $\kappa_1^2=-0.9$ Ry, $\kappa_2^2=-0.2$ Ry, $\kappa_3^2=0.2$ Ry, $\kappa_4^2=0.7$ Ry (four κ).

Number of κ_i^2	1	2	3	4
A_2^0[Ka$_0^{-2}$]	−441	−248	−455	−486
A_4^0[Ka$_0^{-4}$]	−9.8	−9.6	−11.5	−10.8
A_6^0[Ka$_0^{-6}$]	0.22	0.21	0.26	0.23
A_6^6[Ka$_0^{-6}$]	−8.7	−8.6	−7.6	−6.9
V_{cc}(Sm) [10^{21} V m^{-2}]	19.9	8.9	8.4	8.6
μ_{tot} [μ_B]	7.67	7.68	7.75	7.74
ΔE [10^{-3} Ry]	8.69	8.96	9.03	9.05
E_{tot} [Ry]	−34750.312	−34750.314	−34750.365	−34750.376

calculation where we averaged the effective potential within each polyhedral cell before starting the next iteration step. Compared to our full-potential calculations, this type of calculation yielded considerably smaller absolute values for the valence contribution to A_2^0. This explains why the former atomic-sphere calculations which considered only the valence contribution resulted in seemingly correct values of A_2^0. Altogether, it means that a real full-potential calculation without any potential approximation is indispensable.

D. Asphericity of the 4*f* charge density and validity of the two-sublattice model

In all former *ab initio* calculations of A_n^m it was assumed that—in line with the two-sublattice model discussed in Sec. I C—the various parameters of the two-sublattice model are independent of the properties of the $4f$ core (orientation of the moment, asphericity, multiplet state). Accordingly, all calculations we performed for magnetic moments aligning along the crystallographic c axis, and for the $4f$ core a spherically symmetric charge density [Eq. (13)] was inserted. To test this assumption, we have performed the following four calculations (Table V). Calculation A corresponds to the ground state orientation of the $4f$ moment which is along the c axis and antiparallel to the orientation of the transition metal moments, and a spherically symmetric $4f$ charge density is used. In calculation B the orientation of the $4f$ moments is reversed. In calculation C we again consider the ground state orientation, but instead of the spherically averaged $4f$ charge density (13) we insert the aspherical charge density given by Eq. (17). Calculation D corresponds to calculation A with the Sm ion being in the first excited multiplet state ($J=7/2$ instead of $J=5/2$ for the ground state).

From Table V it becomes obvious that most of the parameters (except for the small valence contribution to the magnetic moment of the Sm atom and the related hyperfine field) do indeed not depend strongly on the properties of the $4f$ core. Exceptions are the quantity A_2^0 and the electric field gradient at the Sm site, which are dramatically influenced by the asphericity of the $4f$ core charge density. The main reason is the polarization of the $5p$ states (which are included in the valence band in the calculation for Table V) by the asphericity of the $4f$ core and probably also the modification of the hybridization of the $5p$ states with the other valence states. In calculations which treat the $5p$ states as core states the influence of the $4f$ asphericity therefore probably does not become apparent.

Because the asphericity of the $4f$ charge density is relevant, the value of A_2^0 depends on the orientation of the $4f$ charge density in contrast to the assumption of the two-sublattice model. The comparison of the results from calculations A and C give a feeling for the dependence of A_2^0 on the orientation of the $4f$ moment and hence (via the very strong spin-orbit coupling) of the $4f$ charge density, when the orientation of a $4f$ moment is changed by the application of an external field. As a consequence, the quantities A_2^0 obtained from a multiparameter fit to experimental data based on the assumption that there is no dependence on orientation represent effective parameters which may be different for different experiments. The complication due to the asphericity of the $4f$ charge density arises also for experiments where the orientation of the magnetization is fixed, but the temperature is raised. It is well known (see, for instance, Ref. 44) that the time scale for the thermal orientational disordering of the magnetic moments in a metal is much larger than a typical electronic time scale. As a result, from an electronic viewpoint the system of the $4f$ moments at finite temperature may be envisaged as being stuck for rather long times in a state with fixed and more or less random moment directions at every site, before moving rapidly to another state with modified moment directions, etc. In each state, the local crystal field parameter depends on the local orientation of the respective $4f$ moment. Fitting the experimental data in the usual way therefore again yields effective parameters which should depend on temperature, because the degree of thermal disordering depends on temperature, again in contrast to the assumption of the two-sublattice model. Finally, the situation is even more complicated if we consider systems for which the interaction hierarchy (1) from Sec. I C is not fulfilled (Sm, for instance[45]) so that there is an admixture of higher multiplet states to the ground state of the free R^{3+} ion. From a comparison of calculations A and D one realizes that there should be only a small influence of this admixture as long as a spherically averaged $4f$ charge density is considered. However, it should be noted that the asphericity of the $4f$ charge density is very large for the $J=7/2$ state, so that even a small admixture of this state to the $J=5/2$ ground state would

TABLE V. Test for the dependence of various physical quantities on the properties of the $4f$ core. Shown are the crystal field parameters A_n^m (total as well as valence and lattice contributions), the electric field gradient V_{cc} at the Co sites and the Sm site (without the contribution of the $4f$ core), the valence contribution μ^{val} of the magnetic moment at the Sm site, the local magnetic moments at the two Co sites, the total magnetic moment μ_{total} per unit cell, the contact hyperfine fields B_{hf} and the exchange field B_{ex} describing the intersublattice exchange coupling. For the meaning of the calculations A–D see text. All calculations have been performed with two κ values.

	A	*B*	*C*	*D*
$A_2^0[\mathrm{Ka}_0^{-2}]$				
	−246	−217	−699	−235
Valence	−1447	−1423	−1879	−1439
Lattice	1201	1206	1181	1204
$A_4^0[\mathrm{Ka}_0^{-4}]$				
	−9.6	−9.4	−9.0	−9.6
Valence	0.3	0.5	0.7	0.2
Lattice	−9.9	−10.0	−9.7	−9.9
$A_6^0[\mathrm{Ka}_0^{-6}]$				
	0.22	0.22	0.22	0.22
Valence	−0.09	−0.09	−0.09	−0.09
Lattice	0.31	0.31	0.31	0.31
$A_6^6[\mathrm{Ka}_0^{-6}]$	−8.9	−8.9	−8.8	−8.9
Valence	2.1	2.1	2.2	2.1
Lattice	−11.0	−11.0	−10.9	−11.0
V_{cc}(Sm) $[10^{21}\ \mathrm{V/m}^2]$	8.7	8.4	21.2	8.6
V_{cc}(Co $3g$) $[10^{21}\ \mathrm{V/m}^2]$	6.6	6.3	6.6	6.5
V_{cc}(Co $2c$) $[10^{21}\ \mathrm{V/m}^2]$	−5.0	−5.0	−4.9	−5.0
μ^{val}(Sm) $[\mu_B]$	−0.37	−0.17	−0.37	−0.30
μ (Co $3g$) $[\mu_B]$	1.53	1.50	1.53	1.52
μ (Co $2c$) $[\mu_B]$	1.51	1.48	1.50	1.50
μ_{total} $[\mu_B]$	6.93	7.04	6.91	6.97
B_{hf}(Sm) [T]	−51.7	−12.4	−52.4	−38.8
B_{hf}(Co $3g$) [T]	−19.8	−22.0	−20.0	−20.5
B_{hf}(Co $2c$) [T]	−12.3	−12.6	−12.4	−12.4
B_{ex} [T]	280	280	278	278

probably have a big effect. Because the degree of admixture and hence the asphericity of the $4f$ charge density depend on the orientation of the $4f$ moment, this constitutes a further reason why the experiments yield effective sets of parameters A_n^m which might be different for different experiments.

Altogether, if we want to compare our theoretical results with the experimental data we must also obtain an effective value of A_2^0. The definition of this effective parameter, however, would depend on the experimental situation. The only thing we can do is to determine an effective value which seems to be representative for the variety of various effective values obtained by various experiments. We think that this is obtained by inserting for the calculation of the effective potential a spherical $4f$ charge density according to Eq. (13) instead of the aspherical charge density, and we proceed on this line in all following calculations.

E. Application of the LSDA

In this section the problems related to the application of the LSDA for a determination of the $4f$ core charge density and the valence charge density are discussed.

1. The 4f core

Table VI represents the dependence of A_2^0 on the localization radius $R_{4f,\mathrm{loc}}$ and the logarithmic derivative D_{4f}. For each choice of the two parameters for the $4f$ core we kept the density of all the other charges in the system according to a self-consistent calculation with $R_{4f,\mathrm{loc}}=3.14\ \mathrm{a}_0$ (which is the muffin-tin radius) and $D_{4f}=-\infty$. In the brackets of Table VI we have included the data obtained by a self-consistent calculation for the core and the valence charge densities. It becomes obvious from this table that the values of A_2^0 depend extremely sensitively on the choice of the boundary conditions. For instance, A_2^0 changes by a factor of nearly 3 when going from $R_{4f,\mathrm{loc}}=3.14\ \mathrm{a}_0$, $D_{4f}=-\infty$ to $R_{4f,\mathrm{loc}}=4.10\ \mathrm{a}_0$, $D_{4f}=-4$, although $\langle r^2\rangle_{4f}$ changes only from 0.98 a_0^2 to 1.17 a_0^2. Confining ourselves to $D_{4f}=-\infty$ as outlined in Sec. II B 1, we find for the reasonable range of values for $R_{4f,\mathrm{loc}}$, $3.46\ \mathrm{a}_0 \leqslant R_{4f,\mathrm{loc}} \leqslant 4.10\ \mathrm{a}_0$, a variation in A_2^0 between $-195\ \mathrm{Ka}_0^{-2}$ and $-159\ \mathrm{Ka}_0^{-2}$. (The variation is slightly smaller for the self-consistent calculation for the core and the valence charge densities.) The energy difference ΔE from which we calculate the intersublattice exchange field B_{ex}

TABLE VI. Influence of $R_{4f,\mathrm{loc}}$ and D_{4f} on A_2^0 (in Ka_0^{-2}); see text for the meaning of the numbers in brackets.

		$R_{4f,\mathrm{loc}}[\mathrm{a}_0]$			
		3.14	3.46	3.78	4.10
D_{4f}	$-\infty$	-229	-195	-178	-159
		(-229)	(-210)	(-198)	—
	$-l-1=-4$	-169	-129	-110	-86
	0	-26	43	65	114

(Sec. I) also depends sensitively on the choice of $R_{4f,\mathrm{loc}}$ (for $R_{4f,\mathrm{loc}}=3.14$ a_0 and 3.78 a_0 it is 8.46 mRy and 9.27 mRy, respectively), whereas the higher-order crystal field parameters, the magnetic moments and the magnetic hyperfine fields are virtually independent. According to the suggestion of Steinbeck *et al.*[41] and Novak and Kuriplach[46] (Sec. II B 1), we have included the self-interaction correction in our $4f$ core calculation, for the case $D_{4f}=-\infty$, $R_{4f,\mathrm{loc}}=3.78$ a_0. Instead of our old result of -198 Ka_0^{-2}, we obtained a value of -205 Ka_0^{-2}, demonstrating that the influence of the self-interaction correction is smaller than the influence of different choices for $R_{4f,\mathrm{loc}}$.

We thus have shown that the application of the LSDA for the calculation of the $4f$ core density introduces a big uncertainty of A_2^0. In order to reduce the uncertainty we must take the physically motivated measures described in Sec. II B 1 to obtain reasonable values for the two parameters $R_{4f,\mathrm{loc}}$ and D_{4f}. The remaining uncertainty of about 30 Ka_0^{-2} cannot be considerably reduced by the application of the self-interaction correction.

2. The 4f part of the valence states

According to Sec. II B 2 the application of the LSDA to the calculation of the valence states again requires special physically motivated measures: we must augment the Bessel function j_3 in the muffin-tin sphere by a $4f$ radial function ϕ_{4f} with negative energy, but we should not go to too low values in order to avoid numerical problems. To find a reasonable lower limit we calculate simultaneously the largest component V_{cc} of the electric field gradient tensor at the Sm site (without the contribution from the aspherical $4f$ core), which also depends on the asymmetry of the charge density, but the calculation of which does not involve the folding between the charge densities of the $4f$ core states and the conduction electron states. Therefore, the results do not suffer from the problems with the $4f$ contribution to the valence states discussed in Sec. II B 2, and they are more or less independent of the $4f$ energy parameter except for very low values where numerical problems appear, which is the case for energies smaller than -5 Ry. Table VII represents the data of a three-κ calculation for A_n^m and V_{cc} for the $4f$-energy parameters 0.4 Ry (according to the center of gravity of the occupied valence band, calculation A), -2 Ry (calculation B), and -30 Ry (calculation C). It becomes obvious that calculation A yields totally unrealistic values for A_n^m, and that the very low $4f$ energy parameter of calculation C already deteriorates the electric field gradient. We have investigated the influence of the $4f$ energy parameter on the electric field gradient more thoroughly by a one-κ calculation and found that the results start to deteriorate when going beyond -5 Ry. We thus note that it is reasonable to choose low $4f$ energy parameters to avoid the LSDA problems discussed in Sec. II B 2, but this creates an uncertainty of about 50 Ka_0^{-2} for A_2^0, because there is not strict lower limit for this energy parameter.

TABLE VII. Influence of the $4f$ augmentation energy on the crystal field parameters and the electric field gradient V_{cc} (without the contribution of the $4f$ core) A: 0.4 Ry; B: -2 Ry; C: -30 Ry.

	A	B	C
$A_2^0[\mathrm{Ka}_0^{-2}]$	-1033	-500	-455
$A_4^0[\mathrm{Ka}_0^{-4}]$	3.0	-11.1	-11.5
$A_6^0[\mathrm{Ka}_0^{-6}]$	-0.09	0.27	0.26
$A_6^6[\mathrm{Ka}_0^{-6}]$	26.5	-7.9	-7.6
$V_{cc}(\mathrm{Sm})$ $[10^{21}$ V $\mathrm{m}^{-2}]$	7.9	7.8	8.4

F. Conclusions on the applied calculational method

We have performed in Sec. III for the case of $SmCo_5$ *ab initio* calculations of various parameters occurring in the two-sublattice model of rare-earth–transition-metal intermetallics within the framework of the local-spin-density approximation (LSDA) and the full-potential linear-muffin-tin-orbital theory. Special emphasis is put on the crystal field parameter A_2^0, which appears to be the most sensitive one among the parameters of the two-sublattice model, because it is mathematically given by an integral which involves the folding between the charge densities of the $4f$ states and the conduction electron states. The main objective was to find out whether it is possible to obtain via LSDA charge densities which are sufficiently accurate for the calculation of A_2^0. The main conclusions are the following.

(i) It is absolutely indispensable to include the $5p$ states of the rare-earth atom in the valence band.

(ii) It is also indispensable to perform a full-potential calculation without any spherical approximation for the effective potential.

(iii) The crystal field parameter A_2^0 and the electric field gradient at the Sm site depend strongly on the orientation of the aspherical $4f$ charge density, in contrast to a basic assumption of the two-sublattice model. As a result, the experimental analysis based on this model yields effective parameters A_2^0 which are different for different experiments.

(iv) The application of the LSDA introduces rather large uncertainties for A_2^0, which cannot be totally removed but at least drastically reduced by physically motivated measures.

IV. RESULTS FOR $R\mathrm{Co}_5$

We now report on our results for the series $R\mathrm{Co}_5$. As outlined in Sec. III, it is very difficult to converge the results with respect to all convergence parameters of any calculational method. We therefore have obtained highly accurate results only for $SmCo_5$ and $GdCo_5$. The first material was chosen because it is of high technological importance and

TABLE VIII. Theoretical results for the radial expectation values $\langle r^n\rangle_{4f}$ and the crystal field parameters A_n^m of $SmCo_5$ and $GdCo_5$.

	$SmCo_5$	$GdCo_5$
$\langle r^2\rangle_{4f}[a_0^2]$	0.979	0.868
$A_2^0[Ka_0^{-2}]$	−519	−584
Valence	−1485	−1602
Lattice	966	1018
$A_2^0\langle r^2\rangle_{4f}$[K]	−508	−509
$\langle r^4\rangle_{4f}[a_0^4]$	2.041	1.650
$A_4^0[Ka_0^{-4}]$	−9.8	−10.6
Valence	1.4	0.9
Lattice	−11.2	−11.5
$A_4^0\langle r^4\rangle_{4f}$[K]	−19.9	−17.4
$\langle r^6\rangle_{4f}[a_0^6]$	6.866	5.215
$A_6^0[Ka_0^{-6}]$	0.27	0.31
Valence	−0.08	−0.08
Lattice	0.35	0.39
$A_6^0\langle r^6\rangle_{4f}$[K]	1.86	1.61
$\langle r^6\rangle_{4f}[a_0^6]$	6.866	5.215
$A_6^6[Ka_0^{-6}]$	−8.0	−8.6
Valence	2.9	3.0
Lattice	−10.9	−11.6
$A_6^6\langle r^6\rangle_{4f}$[K]	−54.7	−44.6

because there are *ab initio* calculations[21,47] based on the optimized-linear-combination-of-atomic-orbitals method (OLCAO) for comparison. For $GdCo_5$ there are also calculations based on the OLCAO (Ref. 21) and on the full-potential linearized-augmented-plane-wave method[28,29,48] (FLAPW) for comparison. Because for the spherical $4f$ core of Gd the problem discussed in Sec. III D does not arise our data for the electric field gradient may be directly and quantitatively compared with experiments. On the other hand, for a spherically symmetric $4f$ core there is no magnetic $4f$

TABLE IX. Theoretical results for the electric field gradient V_{cc} at the R site (without the contribution of the $4f$ core) and at the Co sites, the valence contribution $\mu_{\rm loc}^{\rm val}$ of the local magnetic moment at the R site, the local magnetic moments at the Co sites, the total magnetic moment $\mu_{\rm total}$ per formula unit, the magnetic contact hyperfine fields $B_{\rm hf}$ at the R site and the Co sites and the intersublattice exchange field $B_{\rm ex}$, for $SmCo_5$ and $GdCo_5$.

	$SmCo_5$	$GdCo_5$
$V_{cc}(R)$ [10^{21} V/m^2]	8.6	9.8
V_{cc}(Co $3g$) [10^{21} V/m^2]	5.2	5.5
V_{cc}(Co $2c$) [10^{21} V/m^2]	−4.1	−4.4
$\mu_{\rm loc}^{\rm val}(R)$ [μ_B]	−0.37	−0.43
$\mu_{\rm loc}$ (Co $3g$) [μ_B]	1.58	1.59
$\mu_{\rm loc}$ (Co $2c$) [μ_B]	1.55	1.56
$\mu_{\rm total}$ [μ_B]	7.74	0.01
$B_{\rm hf}(R)$ [T]	−31.9	−40.5
$B_{\rm hf}$(Co $3g$) [T]	−19.0	−18.1
$B_{\rm hf}$(Co $2c$) [T]	−11.0	−11.1
$B_{\rm ex}$ [T]	279	239

TABLE X. Same as Table IX, now for R=Pr, Nd, Sm, Gd. Note that the results of this table are not totally converged (see text).

	Pr	Nd	Sm	Gd
$V_{cc}(R)$ [10^{21} V/m^2]	7.0	8.0	9.3	10.8
V_{cc}(Co $3g$) [10^{21} V/m^2]	6.2	6.4	6.7	7.1
V_{cc}(Co $2c$) [10^{21} V/m^2]	−4.8	−4.9	−5.3	−5.3
$\mu_{\rm loc}^{\rm val}(R)$ [μ_B]	−0.32	−0.35	−0.37	−0.43
$\mu_{\rm loc}$(Co $3g$) [μ_B]	1.49	1.51	1.53	1.55
$\mu_{\rm loc}$(Co $2c$) [μ_B]	1.48	1.50	1.52	1.52
$\mu_{\rm total}$ [μ_B]	10.00	10.14	7.66	−0.07
$B_{\rm hf}(R)$ [T]	−29.6	−29.8	−32.9	−38.8
$B_{\rm hf}$(Co $3g$) [T]	−20.5	−20.1	−19.5	−18.5
$B_{\rm hf}$(Co $2c$) [T]	−12.9	−13.0	−12.7	−12.5
$B_{\rm ex}$ [T]	326	311	280	250

anisotropy and hence the crystal field parameters cannot be investigated experimentally. In Sec. IV A we report on highly accurate results for $SmCo_5$ and $GdCo_5$, and on not totally converged data for the series RCo_5 to study the qualitative behavior across the series. In Secs. IV B and IV C we compare with results from other calculations and with experimental data.

A. Results of the present calculations

We first give some computational details for the highly accurate calculations on $SmCo_5$ and $GdCo_5$, referring to Secs. II and III. The calculations were performed for the experimental lattice parameters[49] a=9.4563 a_0 (9.3976 a_0) and c/a=0.7932 (0.7981) for $SmCo_5$ ($GdCo_5$). The Brillouin zone integration was according to Sec. III. The results were satisfactorily converged for 40 k points in the irreducible part of the Brillouin zone and for $(l_B,l_T,2l_W)$=(2,8,10). A three-κ calculation ($\kappa_1^2=-0.9$ Ry for the $5p$ states which are included in the valence band, κ_2^2=0.1 Ry and κ_3^2=0.7 Ry for the $6s$, $6p$, $5d$ states of R and for the $4s$, $4p$, $3d$ states of Co) was performed. The $5s$ states of R and the $3p$ states of Co were treated in a common semicore panel with $\kappa^2=-2.8$ Ry. We used for the augmentation energies the values κ^2 for $l>l_B$ and the respective centers of gravity of the occupied part of the l-projected band for $l\leqslant l_B$, except for the $4f$ states (−2 Ry) and the $6p$ states (D_{6p}=1.5). A spherically

TABLE XI. Same as Table X, now for R=Tb, Dy, Ho, Er.

	Tb	Dy	Ho	Er
$V_{cc}(R)$ [10^{21} V/m^2]	11.3	12.0	12.6	13.3
V_{cc}(Co $3g$) [10^{21} V/m^2]	7.2	7.3	7.3	7.4
V_{cc}(Co $2c$) [10^{21} V/m^2]	−5.3	−5.3	−5.3	−5.5
$\mu_{\rm loc}^{\rm val}(R)$ [μ_B]	−0.38	−0.35	−0.32	−0.30
$\mu_{\rm loc}$ (Co $3g$) [μ_B]	1.55	1.55	1.58	1.57
$\mu_{\rm loc}$ (Co $2c$) [μ_B]	1.51	1.51	1.53	1.53
$\mu_{\rm total}$ [μ_B]	−2.04	−2.99	−2.83	−1.81
$B_{\rm hf}(R)$ [T]	−38.7	−37.8	−33.0	−30.7
$B_{\rm hf}$ (Co $3g$) [T]	−18.7	−19.0	−19.2	−19.3
$B_{\rm hf}$ (Co $2c$) [T]	−12.4	−12.4	−12.6	−12.8
$B_{\rm ex}$ [T]	231	216	203	189

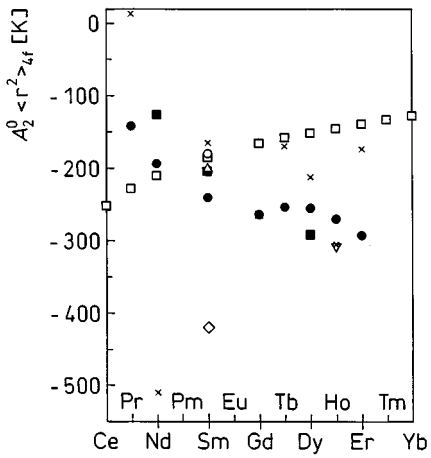

FIG. 3. Comparison of theoretical (not completely converged) and experimental values for $A_2^0\langle r^2\rangle_{4f}$ across the series $R\mathrm{Co}_5$. The full circles (full squares) are the theoretical results for the experimental lattice parameters (for the lattice parameters fixed to the values of GdCo_5). Open triangle up: Givord *et al.* (Ref. 50); open circle: Buschow *et al.* (Ref. 58); open diamond: Sankar *et al.* (Ref. 59); open squares: Radwánski (Ref. 60); crosses: Zhao *et al.* (Ref. 61); open triangle down: Decrop *et al.* (Ref. 63).

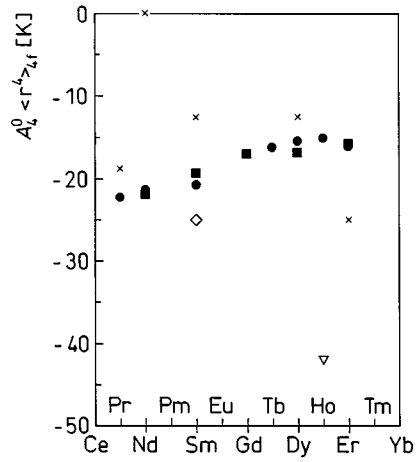

FIG. 4. Comparison of theoretical and experimental values for $A_4^0\langle r^4\rangle_{4f}$ across the series $R\mathrm{Co}_5$. The full circles (full squares) are the theoretical results for the experimental lattice parameters (for the lattice parameters fixed to the values of GdCo_5). Open diamond: Sankar *et al.* (Ref. 59); crosses: Zhao *et al.* (Ref. 61); open triangle down: Decrop *et al.* (Ref. 63).

symmetric $4f$ core according to Eqs. (11)–(15) was assumed for the calculation of the effective potential. It was outlined in Sec. III E 1 that the values of A_2^0 depend extremely sensitively on the choice of the localization parameters D_{4f} and $R_{4f,\mathrm{loc}}$ and that therefore physically motivated measures must be taken to obtain reasonable values for these two parameters. The central idea was to select the parameters in such a way that the expectation values $\langle r^n\rangle_{4f}$ are close to those obtained by the Dirac-Fock calculations[15] for the free R^{3+} ions. For SmCo_5 this was achieved for $D_{4f}=-\infty$ and if the localization radius was slightly larger than the muffin-tin radius. Because it would be a very hard job to optimize the localization parameters separately for all the representatives of the series $R\mathrm{Co}_5$, we insert in the following for all systems the values $D_{4f}=-\infty$ and $R_{4f,\mathrm{loc}}$=muffin-tin radius. The values for $\langle r^2\rangle_{4f}$ and $\langle r^4\rangle_{4f}$ obtained in this way are indeed very close to the Dirac-Fock values, and the values for $\langle r^6\rangle_{4f}$ are slightly smaller.

In Tables VIII and IX we represent our results for the radial expectation values $\langle r^n\rangle_{4f}$ of the $4f$ core, the crystal field parameters A_n^m as well as the products of the two quantities, respectively, and for the local magnetic moments and hyperfine fields, the intersublattice exchange field B_{ex} and the maximum component V_{cc} of the electric field gradient.

To investigate the qualitative trends across the series $R\mathrm{Co}_5$ we reduced the computational effort by confining to a two-κ calculation ($\kappa_1^2=-0.9$ Ry for the $5p$ states, $\kappa_2^2=0.4$ Ry for the other valence states) and by using 20 instead of 40 k points in the irreducible part of the Brillouin zone. The calculations were again performed at the experimental lattice parameters, and it was assumed that the magnetization is aligned to the hexagonal c axis. The results are given in Tables X and XI and Figs. 3–5. Comparing the data for Sm and Gd with those given in Tables VIII and IX it becomes obvious that the confinement to two κ values and 20 k points affects mainly the crystal field parameter A_2^0, whereas the other quantities are considerably less influenced.

Before going into a detailed comparison of our results with other theoretical and experimental data we want to make some general remarks.

(a) For the whole series the lattice contribution to A_2^0 is of the same order of magnitude but of opposite sign than the valence contribution, so that a delicate situation of balance arises.

(b) The quantities $A_6^6\langle r^6\rangle_{4f}$ are generally considerably larger than the quantities $A_4^0\langle r^4\rangle_{4f}$ and therefore cannot be neglected for the analysis of experimental data (in contrast to common use).

(c) The magnetic moments on the two crystallographically different Co sites are very similar, whereas the magnetic hyperfine fields differ drastically. It is often assumed in the literature for the interpretation of Mössbauer experiments

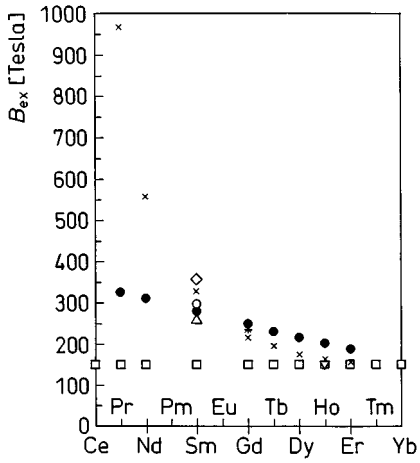

FIG. 5. Comparison of theoretical (full circles) and experimental values for the intersublattice exchange field across the series $R\mathrm{Co}_5$. Meaning of the symbols as in Fig. 2. The star represents the experimental value of Loewenhaupt (Ref. 62).

TABLE XII. Comparison of results from our FLMTO calculations and from OLCAO calculations in the r^4 localization potential (Ref. 21) and in an appropriately defined on-site potential (Ref. 47) including the SIC correction (see text). The quantities $\langle r^n\rangle_{4f,\mathrm{DF}}$ denote the Dirac-Fock expectation values according to Ref. 15. The different signs for A_6^6 result from different definitions of the coordinate systems.

	$SmCo_5$			$GdCo_5$	
	FLMTO	OLCAO-r^4	OLCAO-SIC	FLMTO	OLCAO-r^4
$\langle r^2\rangle_{4f}[a_0^2]$	0.98	1.07	1.02	0.87	0.94
$A_2^0[Ka_0^{-2}]$	−519	−870	−775	−584	−1010
$A_2^0\langle r^2\rangle_{4f}$[K]	−508	−930	−790	−507	−950
$A_2^0\langle r^2\rangle_{4f,\mathrm{DF}}$[K]	−503	−844	−752	−507	−879
$\langle r^4\rangle_{4f}[a_0^4]$	2.04	2.99	2.93	1.65	2.32
$A_4^0[Ka_0^{-4}]$	−10	−13	−13	−11	−13
$A_4^0\langle r^4\rangle_{4f}$[K]	−20	−38	−37	−17	−31
$A_4^0\langle r^4\rangle_{4f,\mathrm{DF}}$[K]	−22	−28	−29	−19	−24
$\langle r^6\rangle_{4f}[a_0^6]$	6.87	17.3	22.2	5.21	12.2
$A_6^0[Ka_0^{-6}]$	0.27	0.35	0.50	0.31	0.4
$A_6^0\langle r^6\rangle_{4f}$[K]	1.9	6	11	1.6	5
$A_6^0\langle r^6\rangle_{4f,\mathrm{DF}}$[K]	2.9	3.7	5.3	2.4	3.1
$\langle r^6\rangle_{4f}[a_0^6]$	6.87	17.3	22.2	5.21	12.2
$A_6^6[Ka_0^{-6}]$	−8.0	8.7	13.1	−8.6	9
$A_6^6\langle r^6\rangle_{4f}$[K]	−55	150	290	−45	100
$A_6^6\langle r^6\rangle_{4f,\mathrm{DF}}$[K]	−85	92	139	−67	70

that the local magnetic moments are proportional to the local magnetic hyperfine fields. As outlined in Ref. 5 this assumption is generally not correct, and this statement is convincingly underpinned by the present results for RCo_5. An analysis of the contributions of core and valence electrons to the local hyperfine fields reveals that the core contributions are indeed very similar for the two Co sites, whereas the valence contributions are not.

B. Comparison with other calculations

The results for the local magnetic moments in $SmCo_5$ and $GdCo_5$ agree quite well with those from OLCAO (Ref. 21) and FLAPW (Ref. 48) calculations. For the Co sites the local magnetic moments are about $0.3\mu_B$ smaller than the values from neutron scattering experiments.[50] Possible reasons are the neglect of the orbital contribution and the fact that the neutron scattering experiments do not resolve the diffuse s- and p-contribution to the spin density (which is negative). The calculated contact hyperfine field at the Gd site agrees well with the values obtained by Coehoorn and Buschow[51] with the augmented-spherical-wave (ASW) method in atomic-sphere approximation, but it differs drastically from the experimental value of −7.4 T.[52] The reason for this discrepancy is unclear.

Our result for the electric field gradient $V_{cc}=9.8\times10^{21}$ V/m^2 at the Gd site is about a factor of 2 smaller than the FLAPW result.[28,29,48] The reason is[53] that in the FLAPW calculations the $5p$ states are treated as semicore states (see remark below) or core states, whereas we included them into the valence band (treating the $5p$ states as semicore states we also obtained a value which was about a factor of 2 larger). The fact that our value agrees excellently with the experimental value[52] of 9.7×10^{21} V/m^2 clearly demonstrates that it is indispensable to include the $5p$ states into the valence band.

For $GdCo_5$ our result of $B_{\mathrm{ex}}=239$ T agrees perfectly with the data from LMTO calculations[54] in atomic-sphere approximation (ASA) (239 T) and from ASW-ASA calculations[55] (239 T). For $SmCo_5$ our value of $B_{\mathrm{ex}}=279$ T differs only slightly from the value obtained by LMTO-ASA calculations[56] (270 T).

For the crystal field parameters, we refrain from comparing our results with those based on the point-charge model, because they depend extremely sensitively on the *ad hoc* assumptions for the point charges (see Sec. I D). We also do not compare with calculations based on the atomic sphere approximation (see Sec. I D): these calculations use a spherical approximation for the potential, although it is absolutely indispensable to consider the true effective potential for a determination of the A_n^m. Furthermore, they consider only the valence contribution and neglect the lattice contribution to A_2^0, although both contributions are large but opposite in sign so that a small total value results (see Table VIII). It remains to compare with the OLCAO calculations[21,47] (Table XII, the separate valence and lattice contributions are not discussed because they are differently defined in the LMTO and OLCAO calculations) and with the FLAPW calculations[28,29,48] (Table XIII).

There are three main differences between the OLCAO and our FLMTO calculations.

(i) Different basis sets are used for the representation of the wave functions.

(ii) The $4f$ core states are treated in a different way (Sec. II B 1). In the OLCAO calculations the $4f$ states are calculated either in a r^4-localization potential[21] or in an appropriately defined on-site potential[47] (the superposition of all on-site potentials yielding the crystal potential). In the latter case the self-interaction correction (SIC) was used (see Sec. II B 1). In the FLMTO calculation the $4f$ states are evaluated in the spherically averaged effective potential for $D_{4f}=-\infty$ at the surface of the muffin-tin sphere around the rare-earth atom.

TABLE XIII. Comparison of results for $GdCo_5$ from our FLMTO calculations and from FLAPW calculations. The quantities $\langle r^n \rangle_{4f,\mathrm{DF}}$ denote the Dirac-Fock expectation values of the free R^{3+} ion according to Ref. 15.

	FLMTO		FLAPW	
	$5p$ valence	$5p$ semicore	$5p$ semicore (Refs. 28 and 29)	$5p$ semicore (Ref. 48)
$\langle r^2 \rangle_{4f}[a_0^2]$	0.868	0.867	0.93	0.984
$A_2^0[\mathrm{Ka}_0^{-2}]$	−584	−717	−824	−724
Valence	−1602	−1747	−1878	
Lattice	1018	1029	1054	
$A_2^0\langle r^2 \rangle_{4f}[\mathrm{K}]$	−507	−622	−763	−707
$A_2^0\langle r^2 \rangle_{4f,\mathrm{DF}}[\mathrm{K}]$	−507	−622	−717	
$\langle r^4 \rangle_{4f}[a_0^4]$	1.650	1.649	2.11	
$A_4^0[\mathrm{Ka}_0^{-4}]$	−10.6	−11.1	−12.8	
Valence	0.9	0.4	−1.4	
Lattice	−11.5	−11.4	−11.4	
$A_4^0\langle r^4 \rangle_{4f}[\mathrm{K}]$	−17.4	−18	−27	
$A_4^0\langle r^4 \rangle_{4f,\mathrm{DF}}[\mathrm{K}]$	−19.2	−20.1	−23	

(iii) Whereas the FLMTO calculations deal with the true effective potential of the crystal, the OLCAO method considers overlapping extended site potentials but for each site potential the intra-atomic asphericity is quenched by azimuthal averaging over the site charge density during the iterations. It has been shown in Sec. III C that it is absolutely indispensable to refrain from any kind of potential approximation: when performing a spherical average of the effective potential in each polyhedral cell at the beginning of each iteration step we arrive at a smaller negative valence contribution and hence at a considerably smaller positive total value of A_2^0.

From Table XII it becomes obvious that the qualitative trends among the different A_n^m are similar in both calculations but that the absolute values of all A_n^m are larger for the OLCAO calculation. As discussed in point (iii) these differences in the absolute values are even increased when adopting in the FLMTO calculation a similar potential approximation as in the OLCAO calculation. The quantitative differences therefore must arise from points (i) and (ii). From these differences it becomes again obvious that the crystal field parameters A_n^m depend extremely sensitively on the computational details.

The comparison of the FLMTO calculations with FLAPW calculations is more natural because both methods deal with the true effective potential and augment the original basis functions by the same type of radial functions in the muffin-tin spheres. Nevertheless, the comparison is aggravated by the following problems.

(i) Because of the use of different basis sets the degree of convergence cannot be compared.

(ii) In Ref. 28 the occupied $4f$ states are treated as core states, but no computational details for this core calculation are given. As demonstrated in Sec. III E 1, the crystal field parameters depend very sensitively on these details. In Ref. 48 the occupied $4f$ states are treated as band states.

(iii) In Sec. III A it has been demonstrated that the results for A_2^0 depend sensitively on the $4f$ augmentation energies. In the published FLAPW calculations the augmentation energies are not given.

(iv) Our FLMTO calculations have shown (see Sec. III A) that it is indispensable to take into account hybridization effects between the $5p$ states and the other valence states. In the FLAPW calculations of Refs. 28, 29 the $5p$ states are treated as semicore states, i.e., they are considered as band states but no hybridization with the valence states is allowed. For a comparison, we have included in Table XIII also our FLMTO results which we obtained by treating the $5p$ states as semicore states (note, however, the slightly different meaning of a semicore calculation in both methods as discussed in Sec. II A). In the FLAPW calculation of Ref. 48 the $5p$ states are treated either as core states or as band states. It does not become clear from the paper whether the $5p$ band states are considered as semicore states or whether hybridization with the valence states is taken into account. There are two hints on the treatment as semicore states. First, as outlined in Sec. II A it is possible to include both the $5p$ and the $6p$ states in a common band if the FLAPW basis set is supplemented by localized orbitals, but no localized orbitals are mentioned in Ref. 48. Second, the change in A_2^0 in Ref. 48 when going from the $5p$ core calculation to the $5p$ band calculation is consistent with the contribution made in Refs. 28, 29 by the $5p$ semicore states both in magnitude and sign.

It becomes obvious from Table XIII that there is a rough agreement between all calculations as long as the $5p$ states are treated as semicore states. When dealing the $5p$ states as valence states in the FLMTO calculation there is still a good agreement for the lattice contributions to A_n^m, but the valence contributions to A_2^0 and hence the total A_2^0 are smaller negative.

C. Comparison with experiments

Basically, two types of experiments have been used for the determination of the crystal field parameters A_n^m and the intersublattice exchange field in the series RCo_5.

(1) High-field measurements at constant temperature. Here a rotation of the magnetization out of the easy direc-

TABLE XIV. Comparison between our theoretical results and experimental data for the crystal field parameters $A_n^m\langle r^n\rangle_{4f}$ and for the intersublattice exchange field B_{ex}. The different signs for A_6^6 result from different definitions of the coordination systems.

	Theory		Experiments			
Ref.		59	50	60	58	61
$A_2^0\langle r^2\rangle_{4f}$[K]	−508	−420	−200±50	−185	−180	−165
$A_4^0\langle r^4\rangle_{4f}$[K]	−20	−25	0±50			−6.3
$A_6^0\langle r^6\rangle_{4f}$[K]	2	1	50±50			0
$A_6^6\langle r^6\rangle_{4f}$[K]	−55	6				0
B_{ex} [T]	279	358	261	151	298	328

tions and a canting between the magnetization of the rare-earth sublattice and the transition-metal sublattice is induced by a strong external magnetic field.[57] The analysis of the experimental data is based on the two-sublattice model, Eqs. (2)–(4), with the Zeeman terms for the interactions between the two sublattice magnetizations and the external magnetic field added.

(2) Measurements of the temperature dependence[50,58–61] of the magnetization and/or the magnetic anisotropy of the rare-earth sublattice. Whereas Eqs. (2)–(4) yield the mean-field energy of the system for *given* thermal averages of the rare-earth spins and the transition-metal spins, the calculation of these temperature dependences with the two-sublattice model starts from the Hamiltonian equivalents to Eqs. (2)–(4) (including the Zeeman terms) obtained by replacing the thermal averages $\langle\hat{S}_R\rangle$ and $\langle\hat{C}_n^m\rangle$ by the respective operators (while keeping the thermal average $\langle\hat{S}_T\rangle$ as function of temperature as input). With the use of the energy eigenvalues obtained from a diagonalization of this Hamiltonian within the subspace of the ground state multiplet J of the free R^{3+} ion the partition function is calculated from which all the thermodynamic information can be obtained. The situation is more complicated in cases where the interaction hierarchy, Eq. (1), is not fulfilled, so that the exchange splitting leads to an admixture of excited multiplet states to the multiplet ground state of the free R^{3+} ion, which depends on the orientation of the $4f$ moment in the intersublattice exchange field B_{ex} produced by the transition-metal sublattice. Then the properties of the $4f$ core, for instance the magnetic moment, depend on the orientation. To account for this admixture of higher multiplet states, the spin-orbit coupling term is added to the above discussed Hamiltonian.[58,59,61] The diagonalization then is carried out within the subspace of the ground state and one or a few excited multiplets.

The following problems which arise for both types of experiments should be kept in mind.

(i) Because the number of parameters in the two-sublattice model is large, the fits to the experimental data are far from being unambiguous, and in general several *ad hoc* assumptions are introduced to facilitate the procedure.[5] Because the higher order crystal field parameters have only a minor effect, the fits are rather insensitive to a variation with respect to these quantities and as a result they can be obtained with large uncertainty only (in Ref. 60 they are totally neglected therefore).

(ii) According to Sec. III D the experiments yield some kind of average effective parameters A_n^m which are different for different experiments (and different from the parameters obtained in the calculations) and which should depend on temperature. Interestingly enough, a temperature dependence of A_2^0 as deduced by fitting the experimental data for the anisotropy constant K_1 at various temperatures was reported by Zhao *et al.*[61]

Of course, these problems for the A_n^m have also an influence on the intersublattice exchange fields, which are determined simultaneously in the above discussed multiparameter fits. An exception is the Gd compound, $GdCo_5$, for which the $4f$ core is spherically symmetric. As a consequence, there is no rare-earth contribution to the magnetic anisotropy, i.e., problem (ii) does not arise and there are only a few fit parameters in the two-sublattice model. Accordingly, for $GdCo_5$ our value of $B_{\mathrm{ex}}=239$ T agrees very well with the value of $B_{\mathrm{ex}}=236$ T obtained by inelastic neutron scattering experiments.[62] In contrast, for $SmCo_5$ all the above discussed problems pertain. Here our value of $B_{\mathrm{ex}}=279$ T is in the wide range of experimental values, spanning from 151 T to 358 T (see Table XIV). Because of the perfect agreement between theory and experiment for $GdCo_5$, we think that our theoretical values for B_{ex} are more reliable than the experimental ones and could be used as fixed input parameters for the data analysis.

The comparison with the experimental results for the A_n^m of $SmCo_5$ is also given in Table XIV. Our theoretical value for A_2^0—while being considerably smaller in absolute value than the one of the OLCAO calculations[21,47]—is in turn considerably larger in absolute value than the experimental values. Table VI shows that the absolute value would decrease a bit when allowing for a further extension of the $4f$ core states, but this alone will certainly not bring down the theoretical value to the range spanned by the experimental data. It is more likely that the discrepancy is related to the problems (i) and (ii) discussed above. The higher order crystal field parameters are either neglected in the experimental analysis or they exhibit a considerable uncertainty because the fits are rather insensitive to a variation of their values. Because they are strongly determined by the lattice contributions (Table VIII), which—in contrast to the valence contributions—depend only weakly on the computational details, we think that our theoretical results are more reliable than the experimental data and could be used as fixed input parameters for the data analysis.

In Figs. 3–5 we compare our theoretical results for the crystal field parameters $A_n^m\langle r^n\rangle_{4f}$ and the intersublattice exchange fields B_{ex} across the series RCo_5 with experimental data. It should be cautioned again that the theoretical data of

these figures (especially for A_2^0) are not completely converged. We nevertheless think that the tendencies across the series are well represented. Our absolute values for $A_2^0\langle r^2\rangle_{4f}$ increase when going through the series from the left to the right. To test whether this tendency results from the variation of the lattice parameters we also performed calculations for which we have fixed the lattice parameters at the values for $GdCo_5$ (full squares in Figs. 3 and 4), yielding the same tendencies. Experimentally, no clear tendency can be observed, the very extensive analysis of Zhao *et al.*[61] arrives at a more or less irregular behavior across the series. [It should be noted that Radwanski[60] started his analysis from the *ad hoc* assumption that A_2^0 is constant across the series, and he arrived at the continuously decreasing absolute values of $A_2^0\langle r^2\rangle_{4f}$ (open squares in Fig. 3) by inserting for $\langle r^2\rangle_{4f}$ the theoretical results from Dirac-Fock calculations[15] for the free R^{3+} ion.] Tables X and XI show that an increase of the absolute values across the series is also found for the electric field gradient of the R site (without the contribution of the R^{3+} ion). It would be interesting to know whether this can be confirmed experimentally.

Figure 4 exhibits theoretical and experimental data for $A_4^0\langle r^4\rangle_{4f}$ across the series. The theoretical absolute values of $A_4^0\langle r^4\rangle_{4f}$ decrease slightly across the series and agree roughly with the experimental data of Zhao *et al.*[61] Figure 5 exhibits theoretical and experimental data for B_{ex} across the series. The decrease of the theoretical values when going from the left to the right is smaller than the decrease of the experimental values reported by Zhao *et al.*[61] (It should be noted that Radwanski[60] started his analysis by the *ad hoc* assumption that B_{ex} is constant across the series.) For $GdCo_5$ where there are no crystal field effects the agreement between theory and experiment is nearly perfect. We therefore assume that the discrepancy for $R \neq$ Gd results from the problems (i) and especially (ii) discussed at the beginning of this section.

ACKNOWLEDGMENTS

We are indebted to Dr. S. Savrasov for supplying us with his FLMTO program as a starting point for the development of our FLMTO code. Most of the calculations were performed at the HLRZ in Jülich.

[1] K. H. J. Buschow, Rep. Prog. Phys. **54**, 1123 (1991).
[2] H. Kronmüller, K.-D. Durst, S. Hock, and G. Martinek, J. Phys. (Paris) Colloq. **49**, C8-623 (1988).
[3] M. S. S. Brooks and B. Johansson, in *Handbook of Magnetic Materials, Vol. 7*, edited by K. H. J. Buschow (Elsevier Science, New York, 1993), p. 139.
[4] R. Coehoorn, in *Electron Theory in Alloy Design*, edited by D. G. Pettifor and A. H. Cottrell (The Institute of Materials, London, 1992), p. 234 ff.
[5] M. Fähnle, K. Hummler, M. Liebs, and T. Beuerle, Appl. Phys. A **57**, 67 (1993).
[6] B. N. Harmon, J. Phys. (Paris) Colloq. **40**, C5-65 (1979).
[7] B. I. Min, H. J. F. Jansen, T. Oguchi, and A. J. Freeman, J. Magn. Magn. Mater. **59**, 277 (1986).
[8] D. J. Singh, Phys. Rev. B **44**, 7451 (1991).
[9] D. M. Bylander and L. Kleinman, Phys. Rev. B **49**, 1608 (1994).
[10] R. Ahuja, S. Auluck, B. Johansson, and M. S. S. Brooks, Phys. Rev. B **50**, 5147 (1994).
[11] W. M. Temmerman, Z. Szotek, and H. Winter, Physica B **186-188**, 903 (1993).
[12] K. N. Clausen, K. A. McEwen, J. Jensen, and A. R. Mackintosh, Phys. Rev. Lett. **72**, 3104 (1994).
[13] G. Zwicknagl, Adv. Phys. **41**, 203 (1992).
[14] R. J. Elliott, in *Magnetic Properties of Rare Earth Metals*, edited by R. J. Elliott (Plenum, London, 1972), p. 1.
[15] A. J. Freeman and J. P. Desclaux, J. Magn. Magn. Mater. **12**, 11 (1979).
[16] M. Yamada, H. Kato, H. Yamamoto, and Y. Nakagawa, Phys. Rev. B **38**, 620 (1988).
[17] R. J. Radwański and J. J. M. Franse, J. Magn. Magn. Mater. **74**, 43 (1988).
[18] H. Stevens, Proc. Phys. Soc. London Sect. A **65**, 209 (1952).
[19] P. T. Hutchings, Solid State Phys. **16**, 227 (1964).
[20] K. Hummler, Ph.D. thesis, University of Stuttgart, 1994.
[21] M. Richter, P. M. Oppeneer, H. Eschrig, and B. Johansson, Phys. Rev. B **46**, 13 919 (1992).
[22] R. Coehoorn, in *Supermagnets, Hard Magnetic Materials*, Vol. 331 of *NATO Advanced Study Institute, Series C*, 1991, edited by G. J. Long and F. Grandjean (Kluwer, Dordrecht, 1991), p. 133.
[23] S. Adam, Gh. Adam, and E. Burzo, J. Magn. Magn. Mater. **61**, 260 (1986).
[24] X.-F. Zhong and W. Y. Ching, Phys. Rev. B **39**, 12 018 (1989).
[25] K. Hummler and M. Fähnle, Phys. Rev. B **45**, 3161 (1992).
[26] K. Hummler, M. Liebs, T. Beuerle, and M. Fähnle, Int. J. Mod. Phys. B **7**, 710 (1993).
[27] M. Fähnle, K. Hummler, T. Beuerle, and M. Liebs, in *Computer Aided Innovation of New Materials II*, edited by M. Doyama, J. Kihara, M. Tanaka, and R. Yamamoto (Elsevier, Amsterdam, 1993), p. 209.
[28] G. H. O. Daalderop, P. J. Kelly, and M. F. H. Schuurmans, J. Magn. Magn. Mater. **104-107**, 737 (1992).
[29] R. Coehoorn and G. H. O. Daalderop, J. Magn. Magn. Mater. **104-107**, 1081 (1992).
[30] M. Liebs, K. Hummler, and M. Fähnle, Phys. Rev. B **46**, 11 201 (1992).
[31] M. Liebs, K. Hummler, and M. Fähnle, J. Magn. Magn. Mater. **124**, L239 (1993).
[32] M. Liebs and M. Fähnle, J. Magn. Magn. Mater. **128**, L8 (1993).
[33] T. Beuerle, M. Liebs, K. Hummler, and M. Fähnle, J. Magn. Magn. Mater. **132**, L1 (1994).
[34] U. von Barth and L. Hedin, J. Phys. C **5**, 1629 (1972); O. Gunnarsson and B. I. Lundqvist, Phys. Rev. B **13**, 4274 (1976); V. L. Moruzzi, J. F. Janak, and A. R. Williams, *Calculated Electronic Properties of Metals* (Pergamon, New York, 1978).
[35] W. Kohn and L. J. Sham, Phys. Rev. **140**, A1133 (1965).
[36] S. Yu. Savrasov and D. Yu. Savrasov, Phys. Rev. B **46**, 12 181 (1992).
[37] O. K. Andersen, Phys. Rev. B **12**, 3060 (1975).
[38] D. Singh and H. Krakauer, Phys. Rev. B **43**, 1441 (1991).
[39] R. M. Moon, W. C. Koehler, J. W. Cable, and H. R. Child, Phys. Rev. B **5**, 997 (1972).

[40] M. S. S. Brooks, L. Nordström, and B. Johansson, J. Phys. Condens. Matter **3**, 2357 (1991).
[41] L. Steinbeck, M. Richter, H. Eschrig, and U. Nitzsche, Phys. Rev. B **49**, 16 289 (1994).
[42] Alternatively, we could also refrain from the 4*f* augmentation, but this would require a considerable modification of the FLMTO code.
[43] P. E. Blöchl, O. Jepsen, and O. K. Andersen, Phys. Rev. B **49**, 16 223 (1994).
[44] B. L. Gyorffy, A. J. Pindor, J. Staunton, G. M. Stocks, and H. Winter, J. Phys. F **15**, 1337 (1985).
[45] K. H. J. Buschow, A. M. van Diepen, and H. W. de Wijn, Solid State Commun. **15**, 903 (1974).
[46] P. Novák and J. Kuriplach, Phys. Rev. B **50**, 2085 (1994).
[47] M. Richter, L. Steinbeck, U. Nitzsche, P. M. Oppeneer, and H. Eschrig (unpublished).
[48] M. Yamaguchi and S. Asano, J. Phys. Soc. Jpn. **63**, 1071 (1994).
[49] K. H. J. Buschow, Rep. Prog. Phys. **40**, 1179 (1977).
[50] D. Givord, J. Laforest, J. Schweizer, and F. Tasset, J. Appl. Phys. **50**, 2008 (1979).
[51] R. Coehoorn and K. H. J. Buschow, J. Magn. Magn. Mater. **118**, 175 (1993).
[52] F. J. van Steenwijk, H. Th. Lefever, R. C. Thiel, and K. H. J. Buschow, Physica **92B**, 52 (1977).
[53] K. Hummler and M. Fähnle, Phys. Status Solidi B **186**, K11 (1994).
[54] T. Beuerle, M. Liebs, K. Hummler, and M. Fähnle, J. Magn. Magn. Mater. **132**, L1 (1994).
[55] J. P. Liu, F. R. de Boer, P. F. de Châtel, R. Coehoorn, and K. H. J. Buschow, J. Magn. Magn. Mater. **132**, 159 (1994).
[56] M. Liebs, K. Hummler, and M. Fähnle, J. Magn. Magn. Mater. **128**, 190 (1993).
[57] J. J. M. Franse, F. E. Kayzel, and N. P. Thuy, J. Magn. Magn. Mater. **129**, 26 (1994).
[58] K. H. J. Buschow, A. M. van Diepen, and H. W. de Wijn, Solid State Commun. **15**, 903 (1974).
[59] S. G. Sankar, V. U. S. Rao, E. Segal, W. E. Wallace, W. G. D. Frederick, and H. J. Garrett, Phys. Rev. B **11**, 435 (1975).
[60] R. J. Radwański, J. Magn. Magn. Mater. **62**, 120 (1986).
[61] T. S. Zhao, H. M. Jin, G. H. Guo, X. F. Han, and H. Chen, Phys. Rev. B **43**, 8593 (1991).
[62] M. Loewenhaupt (private communication).
[63] B. Decrop, J. Désportes, and R. Lemaire, J. Less-Common Met. **94**, 199 (1983).